

1

2 **PP2A inhibitor PME-1 suppresses anoikis, and is associated with**
3 **therapy relapse of PTEN-deficient prostate cancers**

4

5 Christian Rupp¹, Anna Aakula^{1*}, Aleksi Isomursu^{1*}, Andrew Erickson^{2&}, Otto Kauko^{1§},
6 Pragya Shah³, Artur Padzik¹, Amanpreet Kaur¹, Song-Ping Li⁴, Yuba Raj Pokharel¹⁺,
7 Lloyd Trotman⁵, Antti Rannikko⁶, Pekka Taimen^{4,7}, Jan Lammerding³, Ilkka Paatero¹,
8 Tuomas Mirtti², Johanna Ivaska^{1,8}, Jukka Westermark^{1,4#}

9

10 ¹ Turku Centre for Biotechnology, University of Turku and Åbo Akademi University,
11 Turku, Finland

12 ²HUSLAB Laboratory Services, Helsinki University Hospital Medicum and Institute
13 for Molecular Medicine Finland FIMM, University of Helsinki, Helsinki, Finland

14 ³Weill Institute for Cell and Molecular Biology & Meinig School of Biomedical
15 Engineering, Cornell University, Ithaca, NY, USA

16 ⁴Institute of Biomedicine, University of Turku, Turku, Finland

17 ⁵Cold Spring Harbor Laboratory, Cold Spring Harbor, NY 11724

18 ⁶Department of Urology, Helsinki University Central Hospital, Helsinki, Finland.

19 ⁷Department of Pathology, Turku University Hospital, Turku, Finland

20 ⁸Department of Biochemistry, University of Turku, Turku, Finland

21

22 Current addresses:

23 [&]Nuffield Department of Surgical Sciences, University of Oxford, Oxford, United
24 Kingdom

25 [§]Department of Biochemistry, University of Cambridge, Cambridge, UK

26 ⁺Faculty of Life Science and Biotechnology, South Asian University, New Delhi, India

27

28

29 * Equal contribution

30 # Correspondence: jukwes@utu.fi

31

32 **Abstract**

33

34 Identification of novel mechanisms of apoptosis resistance of prostate cancer (PCa)
35 cells has translational importance. Here, we discover that inhibition of tumor
36 suppressor phosphatase PP2A by PME-1 inhibits anoikis (apoptosis in anchorage-
37 independent conditions) in PTEN-deficient PCa cells. PME-1 physically associated
38 with the nuclear lamina and regulated its deformability in PCa cells. In addition, PME-
39 1 deficient cells, with highly deformable nuclear lamina, were particularly vulnerable to
40 anoikis following cell detachment. As a molecular explanation for increased nuclear
41 lamina deformability, PME-1 depletion induced dephosphorylation of nuclear lamina
42 constituents, Lamin-A/C, Lamin-B1, Lamin-B2, LAP2A, LAP2B, and NUP98. PME-1
43 inhibition increased apoptosis also in an *in ovo* tumor model, and attenuated cell
44 survival in zebrafish circulation. Clinically, PCa patients with inhibition of both PP2A
45 and PTEN tumor suppressor phosphatases (PME-1^{high}/PTEN^{loss}), have less than 50%
46 5-year secondary-therapy free patient survival, which is significantly shorter than
47 survival of patients with only PTEN-deficient tumors.

48 In summary, we discover that PME-1 overexpression supports anoikis
49 resistance in PTEN-deficient PCa cells. Further, increased nuclear lamina
50 deformability was identified as plausible target mechanism sensitizing PME-1-
51 depleted cells to anoikis. Clinically, the results identify PME-1 as a novel candidate
52 biomarker for particularly aggressive PTEN-deficient PCa.

53

54 **Keywords:** LMNA, FDPS, AR, ERG, mechanotransduction, ECM

55

56

57

58 **Clinical relevance**

59

60 While organ-confined PCa is mostly manageable, the local and distant metastatic
61 progression of PCa remains a clinical challenge. Resistance to anoikis is critical for
62 PCa progression towards aggressive CRPC. Our data show that PME-1 expression in
63 human PCa cells protects the cells from apoptosis induction in anchorage-
64 independent conditions both *in vitro* and *in vivo*. Clinically, our results identify PME-1
65 as a novel putative biomarker for extremely poor prognosis in PTEN-deficient PCa.
66 Taken together, our results demonstrate novel post-translational regulation of key
67 cancer progression mechanisms, with clear translational implications.

68

69

70 **Introduction**

71

72 Prostate cancer (PCa) is often detected early, and can remain non-aggressive, and
73 non-metastatic, for years. One of the hallmarks of PCa progression towards an
74 aggressive castration-resistant prostate cancer (CRPC) is that PCa cells acquire
75 resistance towards specific type of programmed cell death, anoikis (1). Anoikis is
76 induced in adherent cells by their detachment from other cells, or from surrounding
77 extra-cellular matrix (ECM). Anoikis suppression is not only relevant for indolent PCa
78 cells to acquire anchorage-independence, but also for survival of prostate cancer cells
79 with metastatic potential in circulation (2, 3). Thereby, characterization of mechanisms
80 supporting anoikis resistance of PCa cells could provide novel therapy opportunities
81 for clinical management of PCa by preventing the progression to aggressive and
82 metastatic disease.

83

84 Mechanistically anoikis resistance in PCa has been linked to changes in cell adhesion,
85 cytoskeleton, as well as deregulated intracellular survival pathways (1). Tumor
86 suppressor phosphatase PTEN is inactivated in a large fraction of high grade PCAs
87 (4), and prostate-specific PTEN deletion in a mouse model leads to metastatic PCa
88 (5). Importantly, both PTEN deletion, and hyperactivity of PTEN downstream target
89 AKT increases anoikis resistance (6-8). On the other hand, recent studies in other
90 cancer types indicate for a very delicate balance between nuclear lamina stiffness and
91 anchorage-independence, anoikis resistance, and cell migration. Whereas cell
92 migration in three dimensional contexts requires a sufficiently deformable nuclear
93 lamina to allow passage through physical restrictions (9-11), too deformable nuclei

94 may limit cancer cell survival especially in anchorage-independent conditions (9, 12-
95 15). Of nuclear lamina proteins, particularly inhibition of both Lamin-A/C and Lamin-
96 B1 sensitizes cells to DNA damage and apoptosis (16, 17). Further, Lamin A/C
97 deficiency reduces circulating tumor cell resistance to fluid shear stress (12), and to
98 sensitize cells to anoikis (14). Together, this evidence highlights the emerging
99 importance of nuclear lamina deformability in defining anoikis resistance. However,
100 the post-translational regulation of nuclear lamina deformability, or its importance for
101 PCa progression is poorly understood.

102

103 Protein phosphatase 2A (PP2A) is another tumor suppressor phosphatase, in addition
104 to PTEN, that is commonly inactivated in PCa. PP2A functions as a trimeric protein
105 complex composed of the scaffolding A-subunit, catalytic C-subunit, and a number of
106 regulatory B-subunits (18, 19). In most human cancers, PP2A is inactivated by
107 overexpression of PP2A inhibitor proteins such as CIP2A, SET or PME-1 (20-22),
108 whereas in a small percentage of cancers it is inhibited by either loss of specific B-
109 subunits or by inactivating mutations in A-subunits (18). Overexpression of PP2A
110 inhibitor protein CIP2A clinically associates with CRPC (26), and inhibition of both
111 CIP2A and SET inhibits malignant growth of PCa cells, including PTEN-deficient
112 CRPC cells (26, 27). In contrast, role for PME-1 in PCa is currently unknown.
113 Interestingly, PP2A, CIP2A and PME-1 all physically associate with Lamin-A/C (28-
114 30), and PP2A B-subunit PPP2R2A promotes nuclear lamina reformation after mitosis
115 (31). However, the specific phosphorylation sites regulated by PP2A on nuclear lamina
116 constituents, and the oncogenic relevance of PP2A's potential role on nuclear lamina
117 regulation, remain to be identified.

118

119 In this study, we demonstrate that PP2A inhibitor protein PME-1 (21), that has not
120 been previously implicated in PCa, has a critical role in anoikis suppression of PTEN-
121 deficient PCa cells both *in vitro* and *in vivo*. PME-1 regulates phosphorylation of
122 several nuclear lamina proteins. Consequently, PME-1-depleted PCa cells have
123 significantly more deformable nuclei, and those cells are hypersensitized to cell death
124 under anoikis-inducing conditions. Clinically, PCa tumors with inhibition of both tumor
125 suppressor phosphatases PTEN (genetic deletion), and PP2A (PME-1
126 overexpression), had significantly shorter relapse-free survival. Finally, PME-1
127 overexpression suppressed anoikis and promoted Lamin-A/C phosphorylation in
128 genetically defined PTEN-deficient cell model.

129

130 **Result**

131

132 **PME-1 promotes anchorage-independent growth of prostate cancer cells.**

133

134 Based on recent reports of potential clinical relevance of PP2A inhibition in human
135 PCa (23-27, 32, 33), but lack of studies related to PME-1, we tested the impact of
136 PME-1 depletion on colony growth of two PTEN-deficient PCa cells lines PC-3 (PTEN
137 null) and DU-145 (PTEN heterozygous). PME-1 silencing by two independent siRNA
138 sequences did not affect colony growth of either of the cell lines in 2D adherent culture
139 conditions (Figure 1A). However, PME-1 silencing did decrease anchorage-
140 independent growth on soft agar assay in both PC-3 and DU-145 cells (Figure 1B). To
141 further assess whether PME-1 is particularly relevant for growth under low-attachment
142 conditions, we performed spheroid growth assays on low attachment plates. PME-1
143 inhibition prevented the growth of floating PC-3 spheroids (Figure S1A), and reduced
144 cell viability in these conditions (Figure 1C). Furthermore, we observed a strong
145 synergy between PME-1 inhibition and low-attachment culture conditions in PARP
146 cleavage (Figure 1D), indicating that apoptotic cell death contributes to decreased
147 anchorage-independent growth of these cells. In order to rule out the possibility of
148 siRNA off-target effects, we created a PC-3 PME-1 knock-out (KO) cell line by
149 CRISPR/Cas9. Comparison of cleaved PARP expression between Cas9
150 overexpressing control cells with and without non-targeting gRNA (lanes 1-3), a pool
151 of PME-1 gRNA transfected cells (lane 4), and a single cell subclone of PME-1
152 targeted cells (lane 5), demonstrated dose-dependent apoptosis induction upon PME-
153 1 loss in cells following detachment (Figure 1E). PME-1 KO cells also displayed
154 significantly reduced cell viability on low attachment plates (Figure S1B).

155

156 Previously, it was shown that non-transformed cells succumb to anoikis-type cell death
157 when plated on soft substrates, whereas cancer cells do not die under same conditions
158 (34). In order to test whether PME-1 expression is part of the apoptosis resistance
159 mechanism also for cancer cells on low stiffness matrix, either control or PME-1 siRNA
160 transfected PC-3 cells were plated on low- (0.5 kPa) or high (50 kPa)-stiffness
161 hydrogels functionalized with ECM components (fibronectin and collagen I).
162 Consistently with published results with other cancer cells (34), control PC-3 cells
163 showed a very small increase in PARP cleavage on low stiffness (Figure 1F).
164 Importantly, PME-1 depletion sensitized the cells to apoptosis induction selectively in
165 low-stiffness conditions (Figure 1F).

166

167 Together these data demonstrate that PME-1 protects human PCa cells from
168 apoptosis when cells are exposed to anchorage independence, or to low tissue
169 stiffness.

170

171 **PME-1 supports *in vivo* anoikis resistance and survival of prostate cancer cells
172 in circulation**

173

174 To test the *in vivo* relevance of PME-1-mediated inhibition of PCa cell anoikis, we used
175 either scrambled or PME-1 siRNA transfected PC-3 cells in a chicken embryo
176 chorioallantoic membrane (CAM) assay (Figure 2A). Tumors formed by PME-1
177 depleted cells were overall more translucent, suggesting decreased tumor growth
178 (Figure S1C). In accordance with anoikis suppressing activity of PME-1, histological
179 analyses of dissected tumors revealed increased TUNEL positivity in tumors derived

180 from PME-1 siRNA transfected cells (Figure 2B,C). Tumor suppression was further
181 confirmed by reduced number of Ki-67 positive cells in tumors derived from PME-1
182 siRNA transfected cells (Figure 2B,C).

183

184 To test whether high PME-1 expression would suppress cell death also in response to
185 flow-shear stress, and in disseminated PCa cells, we examined survival of control and
186 PME-1 depleted PC-3 cells in zebrafish circulation using recently described
187 experimental setting (35). In short, cell suspensions of scrambled and PME-1 siRNA
188 transfected cells were microinjected into the common cardinal vein of the embryo
189 using a glass microinjector and successfully transplanted embryos were selected to
190 the experiment. After overnight incubation the embryos were imaged by fluorescence
191 stereomicroscopy (Figure 2D). Quantitation of fluorescent tumor cells per zebrafish
192 embryo demonstrated that PME-1 significantly supported survival of circulating PC-3
193 cells (Figure 2E).

194

195 Together, these results validate the *in vivo* relevance of PME-1-mediated anoikis
196 resistance in PCa cells.

197

198 **PME-1 associates with the nuclear lamina and regulates nuclear deformability**

199

200 PME-1-mediated support of cancer cell survival in other cell types has been mostly
201 attributed to increased AKT activity (36). However, we could not detect any consistent
202 effects on AKT phosphorylation by PME-1 silencing in PC-3 cells either *in vitro* or *in*
203 *vivo* (Figure S2A,B). As a reason for these discrepant results, it is possible that PTEN
204 loss in PC-3 is alone sufficient for activation of AKT, and PME-1 has no further effect.

205 Also, the levels of MYC, which is another oncogenic PP2A target relevant for PCa,
206 were not affected by PME-1 silencing (Figure S2A,B).

207

208 To seek for alternative targets for PME-1-mediated anoikis suppression in prostate
209 cancer cells, we focused on recently identified association of PME-1 with nuclear
210 lamina. PME-1 was shown to interact with both Lamin-A/C, and with nuclear lamina-
211 associated farnesylase FDPS (30, 37). Further, siRNA-mediated inhibition of either
212 PME-1, or Lamin-A/C, or FDPS, resulted in comparable loss of viability phenotype in
213 PC-3 cells (30). The rationale of nuclear lamina regulation being a potential
214 mechanism protecting PME-1 expressing cells from anoikis is based on recent studies
215 demonstrating that increased nuclear lamina deformability sensitizes cancer cells to
216 apoptosis and anoikis (9, 12, 13). More specifically, inhibition of both Lamin-A/C and
217 Lamin-B1 sensitizes cells to DNA damage and apoptosis (16, 17).

218

219 We confirmed the physical association of PME-1 with Lamin-A/C in PC-3 cells by
220 proximity ligation assay (PLA) (Figure 3A). The specificity of PLA signal was confirmed
221 by clear loss of signal in PME-1 depleted cells. To identify potential PME-1-regulated
222 PP2A target phosphorylation sites on nuclear lamina, we re-analyzed recently
223 reported LC-MS/MS phosphoproteome analysis data from PME-1 depleted cells (28).
224 Notably, PME-1 inhibition was found to result in dephosphorylation of several nuclear
225 lamina constituents. Specifically, PME-1 inhibition resulted in dephosphorylation of
226 Lamin-A/C, Lamin-B1 and B2, NUP98, and of chromatin anchoring proteins LAP2A
227 and LAP2B (Figure 3B), without altering cell cycle distribution (data not shown). As
228 many of the regulated proteins impact nuclear deformability, the effects of PME-1

229 depletion on nuclear deformability was directly assessed by subjecting the control and
230 PME-1 knock-out cells to a micropipette aspiration experiment as described previously
231 (38). Indeed, PME-1 KO cells had significantly more deformable nuclei based on
232 micropipette aspiration experiment (Figure 3C,D). Interestingly, both cell lines show a
233 similar slope for the deformation over longer time periods and mostly vary in their initial
234 deformation (Figure 3D), indicating differences in their elastic properties.

235

236 Although the increased nuclear deformability in PME-1 negative cells potentially
237 involves dephosphorylation of all identified nuclear lamina components (Figure 3B),
238 Lamin-A was the only protein for which there were phosphoantibodies available for the
239 PME-1-regulated sites. From the original PP2A LC-MS/MS phosphoproteome data
240 (28), we identified 8 Lamin-A/C phosphopeptides, with 10 phosphosites, that were
241 regulated negatively by PME-1 depletion, and positively by inhibition of the PP2A
242 scaffold subunit PPP2R1A (Figure S3A). Out of these sites, currently there are
243 phosphoantibodies available for Serine 22 (S22) and S392 and these were used to
244 validate nuclear lamina phosphorylation regulation by PME-1 under anoikis-inducing
245 conditions.

246

247 Recent studies using hematopoietic stem cells have demonstrated increase in S22
248 phosphorylation of Lamin-A/C in response to loss of cell adhesion (39). We could
249 confirm this phenotype also in scrambled siRNA transfected PC-3 cells by trypsin-
250 induced detachment (Figure 3E). Importantly, the cells in which PME-1 expression
251 was inhibited, either by siRNA, or by knockout, showed clearly lower levels of Lamin-
252 A/C serine 22 phosphorylation up to 210 minutes of follow-up after detachment (Figure
253 3E and S3B). Importantly, similar results were observed with serine 392

254 phosphorylation (Figure 3E). Further, inhibition of Lamin-A/C serine 22
255 phosphorylation was sustained for up to 24 hours in PME-1 depleted cells that were
256 detached and re-plated on low stiffness hydrogel matrix (Figure 3F and S3C). To
257 further strengthen the PP2A-dependence of Lamin-A/C phosphorylation regulation by
258 PME-1, we carried out a rescue experiment by co-depletion of the PP2A B-subunit
259 PPP2R2A. PPP2R2A mediates PME-1 effects in human glioma cell therapy resistance
260 (40), and it is deleted in 8% of human prostate cancers (24, 25) (Figure S3D).
261 Reassuringly, co-depletion of PPP2R2A prevented inhibition of Lamin-A/C
262 phosphorylation in detached PME-1 depleted cells (Figure S3E,F).

263

264 Given that Lamin-A/C is the major determinant of nuclear lamina elasticity (14), and
265 that PME-1 regulated several Lamin-A/C phosphorylation sites, we used Lamin-A/C
266 phosphorylation mutants to study the functional relevance of this phosphorylation
267 regulation for anoikis resistance. To this end we used PC-3 cells in which endogenous
268 Lamin-A/C expression was suppressed by shRNA targeting the 3'UTR of Lamin-A/C
269 gene (Figure 3G), and the cells were transiently transfected with either wild-type
270 Lamin-A/C or with a Lamin-A/C mutant with both serine 22 and 392 mutated to alanine
271 (Figure S3G). Supportive of the importance of Lamin-A/C S22 and S392
272 phosphorylation for survival in low attachment conditions, re-expression of phospho-
273 deficient Lamin-A/C mutants reduced the survival of cells with low endogenous Lamin-
274 A/C levels, whereas overexpression of the WT Lamin-A/C resulted in a modest
275 increase in survival (Figure 3H).

276

277 These results identify nuclear deformability as a novel PP2A-regulated phenotype in
278 cancer cells. Together with data linking nuclear lamina deregulation to increased

279 apoptosis susceptibility (9, 12, 13, 16, 17), PME-1-mediated regulation of nuclear
280 lamina is a plausible mechanism by which PME-1 negative prostate cancer cells are
281 protected from anoikis (Fig. 4H).

282

283 **PME-1 overexpression in prostate cancer associates with PTEN loss and with**
284 **therapy relapse**

285

286 To evaluate the clinical relevance of PME-1 in human PCas, PME-1 protein
287 expression, and its clinicopathological associations, were evaluated in PCa tissue
288 microarray (TMA) material consisting of 358 patients treated primarily with radical
289 prostatectomy in the Helsinki University Hospital between 1983 and 1998. The clinical
290 cohort has been previously described in detail (41, 42) (see also Table S1 for
291 demographics).

292

293 The specificity of the PME-1 antibody for immunohistochemical (IHC) stainings has
294 been validated previously (43). PME-1 expression was scored using 4-tier scale of
295 negative, low, intermediate and strong expression (Figure 4A). As each patient had
296 three cancerous cores in the TMA, the maximum values of PME-1 scores were used
297 and each patient was dichotomized as either high or low (strong vs. negative to
298 intermediate staining). In the correlation analysis with clinical variables, strong PME-1
299 protein expression correlated with higher Grade group and advanced stage (Table 2).
300 We also correlated PME-1 status with previously assessed PTEN, ERG and AR
301 status. Notably, high PME-1 expression statistically significantly associated with
302 complete PTEN loss, but also with ERG positivity and high AR expression status
303 (Figure S4A). Further assessment of patient populations based on this data, and

304 regarding predicted activity status of PTEN and PP2A, defined a subcohort of
305 approximately 8% of patients with impaired activities of both tumor suppressors
306 (Figure 4B).

307

308 Survival analysis showed that the patients with high PME-1 expression have
309 shortened disease-specific survival, although this was not statistically significant
310 (Figure S4B). However, patients with high PME-1 expression had statistically
311 significantly shorter time to secondary therapies after primary treatment (i.e. relapse
312 free survival) (Figure 4C). Most importantly, the patients with both complete loss of
313 PTEN and high PME-1 expression defined a remarkably aggressive patient population
314 with less than 50% 5-year secondary-therapy free survival (Figure 4D). Similar, albeit
315 less prominent cooperative effects were observed with PME-1 overexpression and
316 with either ERG or AR expression (Figure 4E and S4C).

317

318 Together with functional data these observations indicate clinical relevance for PME-
319 1-mediated anoikis suppression in PTEN-deficient PCa. To confirm this functional
320 association of two tumor suppressor phosphatases in a more genetically defined
321 model system, PME-1 cDNA construct was stably transfected to PTEN/p53 knock-out
322 mouse embryonic fibroblasts (MEFs). In accordance with siRNA and Crispr/Cas
323 results, overexpression of PME-1 in PTEN/p53 knock-out MEFs prevented PARP
324 cleavage upon 24h incubation in low attachment conditions (Figure 4F). Moreover,
325 PME-1 overexpression increased Lamin-A/C phosphorylation in PTEN/p53 knock-out
326 MEFs consistently with other results (Figure 4G).

327

328

329 **Discussion**

330 During tumor growth, and particularly during invasion and metastatic spread, cancer
331 cells are exposed to varying levels of stress. Particularly detachment of cells from
332 other cells, and from ECM, makes cells vulnerable to anoikis induction. Thereby,
333 mechanisms that inhibit cancer cell anoikis facilitate local tumor spreading, and
334 eventually metastasis. Here we report high expression of PP2A inhibitor PME-1 as a
335 anoikis resistance mechanism in PTEN-deficient PCa cells. The clinical relevance of
336 anoikis suppression by PME-1 is supported by association of patient population with
337 PTEN^{loss}/PME-1^{high} tumors with remarkably short time to secondary therapies.

338

339 Although anoikis suppression is a generally relevant mechanisms for tumor
340 progression, it may have particular clinical importance in slowly progressing cancers
341 such as PCa where cancers can be diagnosed in indolent phase, and there is a strong
342 need to be able to both predict and inhibit the likelihood of disease progression (4).
343 Previously anoikis resistance in PCa cancer has been linked mechanistically to
344 regulation of cell adhesion, cytoskeleton (1), PTEN inhibition (6), and AR activity (44).
345 In addition to remarkable clinical connection between PTEN and PME-1 (Figure 4D),
346 we found that low PME-1 and AR expression tumor expression was associated with
347 significantly prolonged therapy-free survival (Figure 4E). These results are particularly
348 interesting given that pharmacological PP2A reactivation leads to AR degradation, and
349 to significant PCa tumor regression (32), corroborating situation seen in the less
350 aggressive tumors with high PP2A activity (PME-1^{low}) and low AR expression (Figure
351 4E).

352

353 PTEN and PP2A have both been identified independently as PCa tumor suppressor
354 phosphatases (4, 23, 27, 33), but the clinical relevance of their co-operation has not
355 been studied thus far. Here, we demonstrate an important role for PME-1-mediated
356 PP2A inhibition in anoikis suppression in various PTEN-deficient models. Clinically,
357 simultaneous inhibition of both tumor suppressor phosphatases was associated with
358 very aggressive disease with high propensity for early disease relapse (Figure 4D). As
359 PTEN deficiency has also been shown to promote anoikis resistance of PCa cells (6),
360 the tumor cells with inhibition of both PP2A and PTEN are assumed to be particularly
361 well protected from anoikis, and we hypothesize that this is likely to contribute to
362 observed clinical aggressiveness of these cancers. Mechanistically PTEN-mediated
363 anoikis resistance is mediated by AKT signaling (6, 7), whereas we showed that PME-
364 1 depletion had no effect on AKT phosphorylation (Figure S3A,B). The non-
365 overlapping downstream mechanisms for PTEN and for PME-1 in anoikis suppression
366 further explains their synergetic actions. As PTEN genetic status can be routinely
367 evaluated in current clinical PCa diagnostic practice (4), our results indicate diagnostic
368 utility of assessment of PME-1 status on patients with complete PTEN loss. Although
369 further studies are clearly needed to validate these conclusions, our results indicate
370 that patients with PTEN^{loss}/PME-1^{high} tumors might benefit from more intensive follow-
371 up, and/or from more aggressive therapies as the first, and second line treatments.

372
373 PME-1 expression protected PCa cells from anoikis in various anchorage-independent
374 conditions (soft agar, trypsin-detachment), or under conditions with low ECM-cell
375 mechanotransduction (low adhesion plates, low stiffness). We also demonstrate for
376 the first time that PP2A modulation regulates nuclear deformability. Our results are
377 fully consistent with the published model that different levels of nuclear lamina

378 deformability support different cellular functions (Figure 4H). Whereas a stiff lamina
379 prevents cell migration through physical restrictions, a highly deformable lamina
380 renders cells vulnerable to apoptosis induction by low tissue tension, and fluid stress
381 (9, 12, 15, 17, 45). Further, a recent study indicates that aggressive prostate cancer
382 cells such as PC-3 and DU-145 have softer nuclei than immortalized benign prostate
383 epithelial cells (46). As we demonstrate an important role for PME-1 in preventing
384 further softening of the nuclear lamina in PC-3 cells, and link this to the anoikis
385 suppression, we speculate that during cellular transformation nuclear lamina becomes
386 softened to allow cell migration, whereas PME-1 overexpression in cancerous cells
387 prevents softening of their nuclear lamina to the levels that would make them
388 sensitized to anoikis (Figure 4H). Although alternative mechanisms downstream of
389 PME-1 may contribute to its anoikis suppressing function, we emphasize that nuclear
390 lamina deformability regulation may have been overlooked as a critical mechanism
391 supporting viability of PCa cells during their progression towards full malignancy.
392 Importantly, although Lamin-A/C phosphor-antibody analysis was used to validate
393 PP2A-mediated regulation of nuclear lamin proteins, it is very likely that PP2A-
394 mediated dephosphorylation of other detected nuclear lamina proteins are important
395 for both the observed nuclear deformability phenotype. In addition to phosphotargets
396 of PME-1, PME-1 also interacts with a FDPS(30) which contributes to farnesylation of
397 Lamin-A/C, B1 and B2(37). Therefore also this nuclear lamina-associated PME-1
398 protein interaction may contribute to the observed nuclear deformability regulation.
399 The molecular mechanisms by which too deformable nuclei sensitizes apoptosis is
400 currently under debate. As nuclear chromatin is tightly connected with lamina (47),
401 and DNA arrangements sensitize to apoptosis, it is possible that dephosphorylation of

402 chromatin arranging LAP2A/B proteins may contribute to anoikis induction in PME-1
403 negative cells under low attachment conditions.

404

405 Together these results identify anoikis resistance as a candidate mechanism by which
406 PME-1-mediated PP2A inhibition promotes malignant progression of prostate cancer.

407 Together with emerging orally bioavailable PP2A reactivating compounds with
408 profound antitumor activity in *in vivo* PCa models (32), these results clearly emphasize
409 future importance of comprehensive understanding of PP2A biology for management
410 of aggressive prostate cancer patients. The results also identify PME-1 as a potential
411 biomarker for improved stratification and better therapy response among PCa patients
412 with complete PTEN loss. Together with other findings, results further indicate that
413 diagnostic PME-1 evaluation from PTEN negative tumors may help to identify patients
414 that would benefit from more intensive follow-up after therapy.

415

416

417

418

419

420

421

422

423

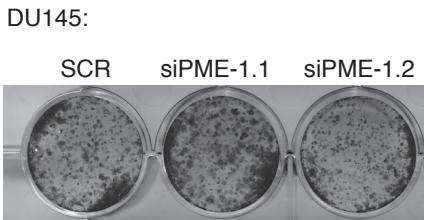
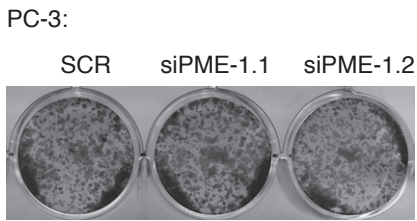
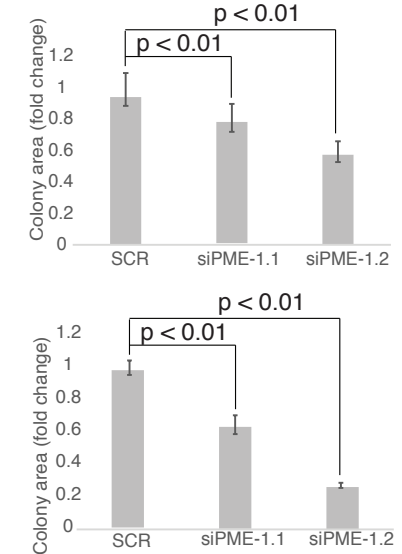
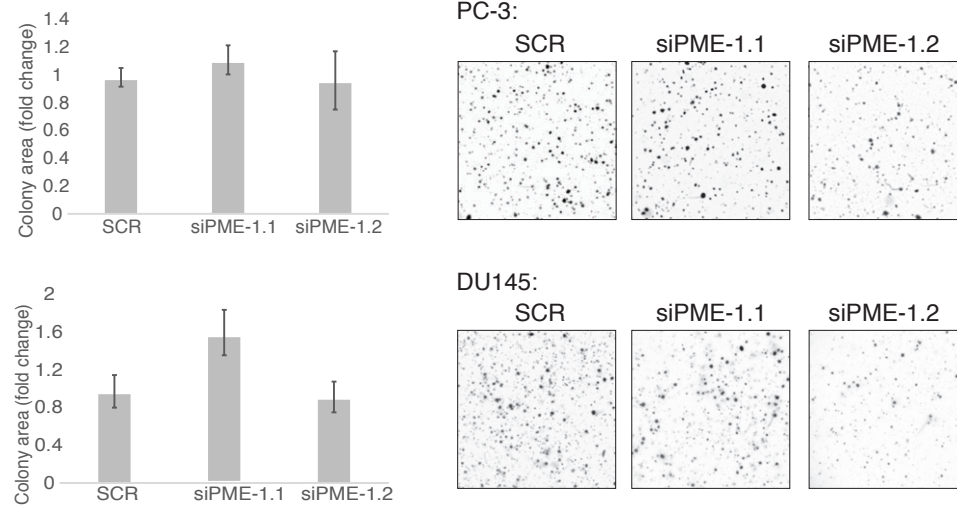
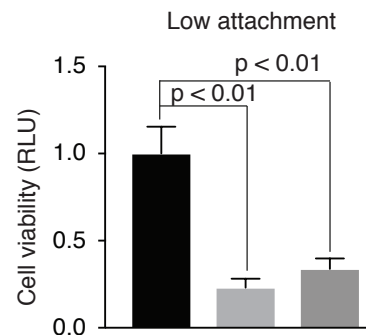
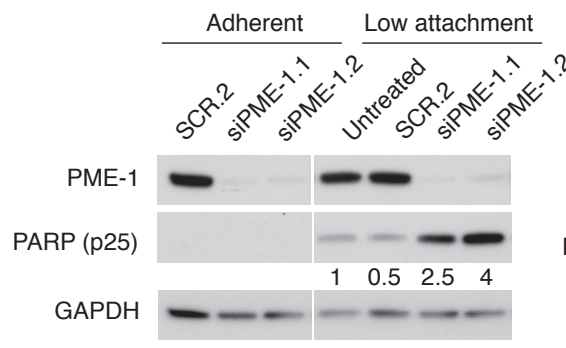
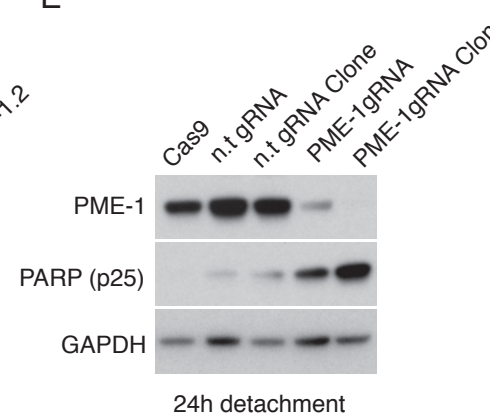
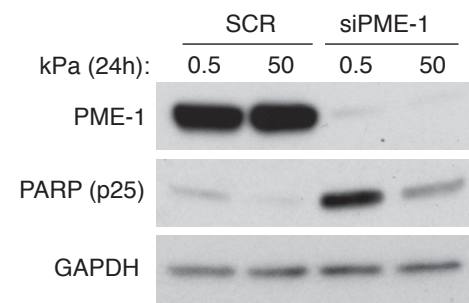
424

425 **Acknowledgements**

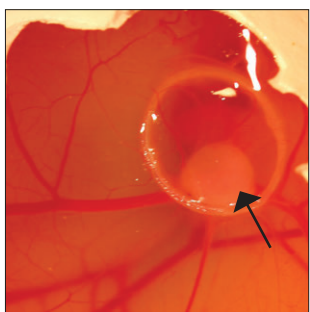
426

427 We thank The Proteomics and The Cell Imaging Core at Turku Centre for
428 Biotechnology supported by the University of Turku and Biocenter Finland, for
429 technical assistance. Taina Kalevo-Mattila is thanked for excellent technical help. This
430 work was supported, in part, by grants from Academy of Finland (J.W, J.I), Academy
431 of Finland CoE for Translational Cancer Research (J.I), Sigrid Juselius Foundation
432 (J.W, J.I.), and the Finnish Cancer Organization (J.W, J.I., P.T.), the National Institutes
433 of Health [R01HL082792 and U54CA210184 to JL], the Department of Defense Breast
434 Cancer Research Program [Breakthrough Award BC150580 to JL], and the National
435 Science Foundation [CAREER Award CBET-1254846 to JL]. This work was
436 performed in part at Cornell NanoScale Facility (CNF), an NNCI member supported
437 by NSF Grant NNCI-1542081. A.I. has been supported by the University of Turku
438 Doctoral Programme in Molecular Life Sciences (DPMLS).

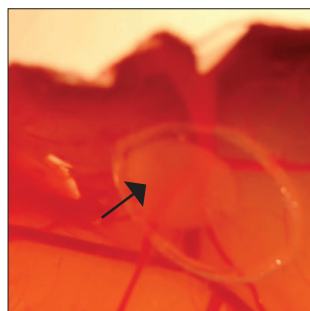
439

A**B****C****D****E****F****Figure 1**

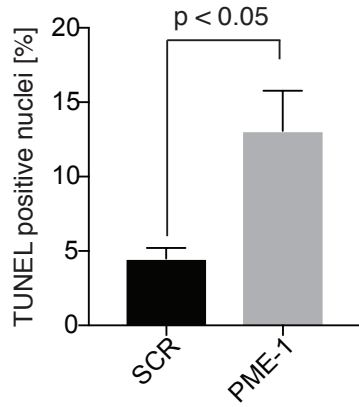
A



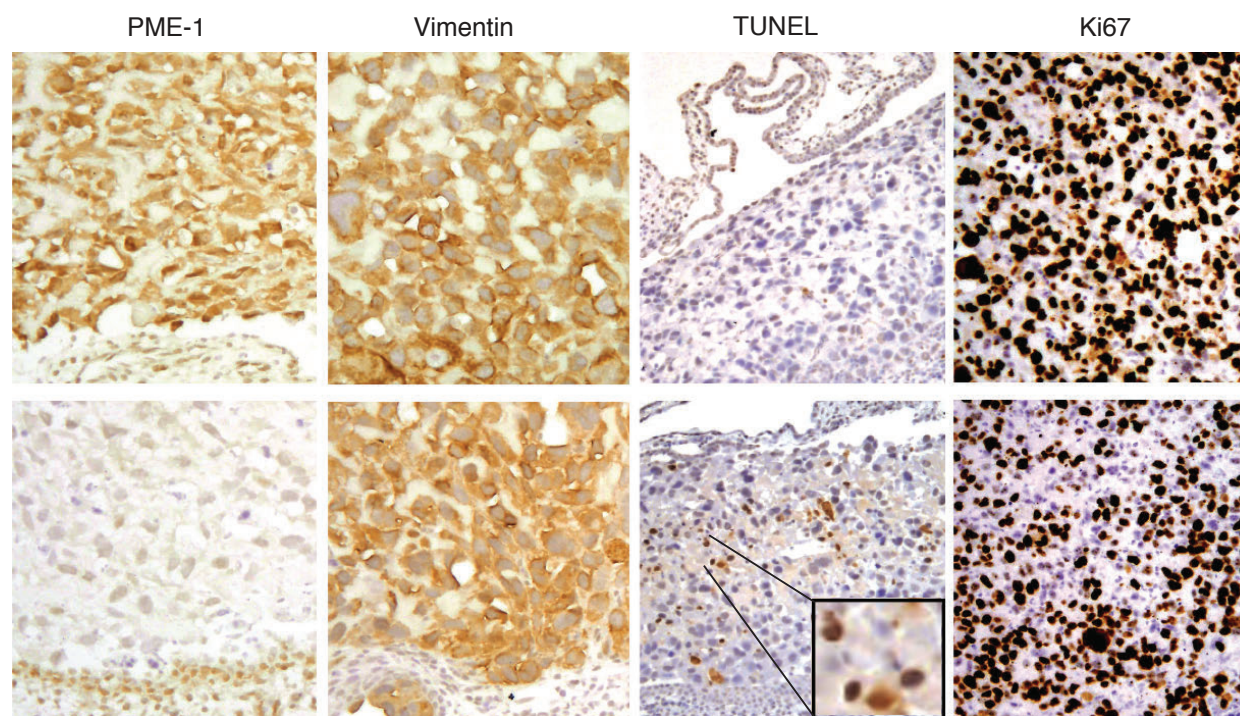
siPME-1



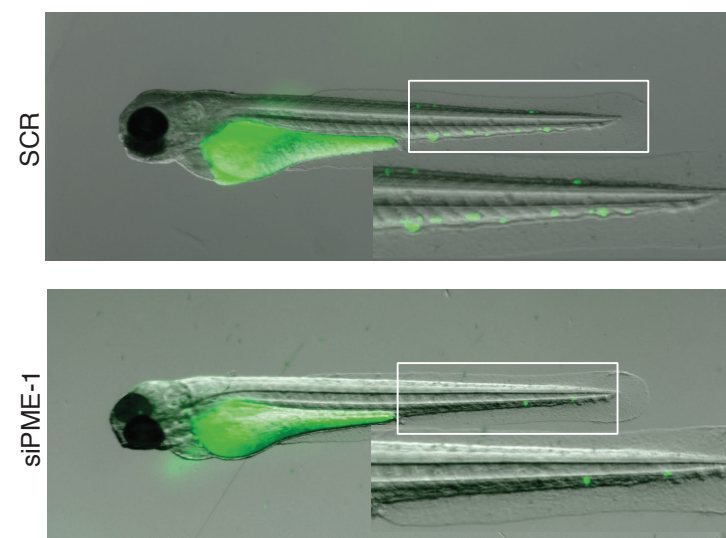
C



B



D



E

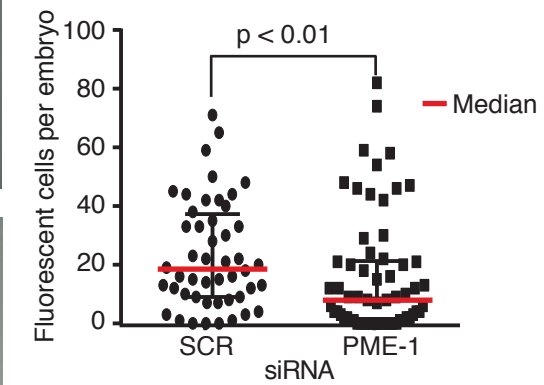
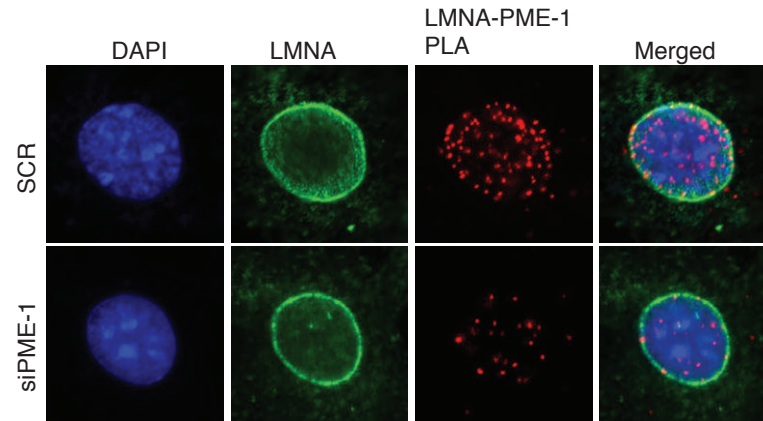
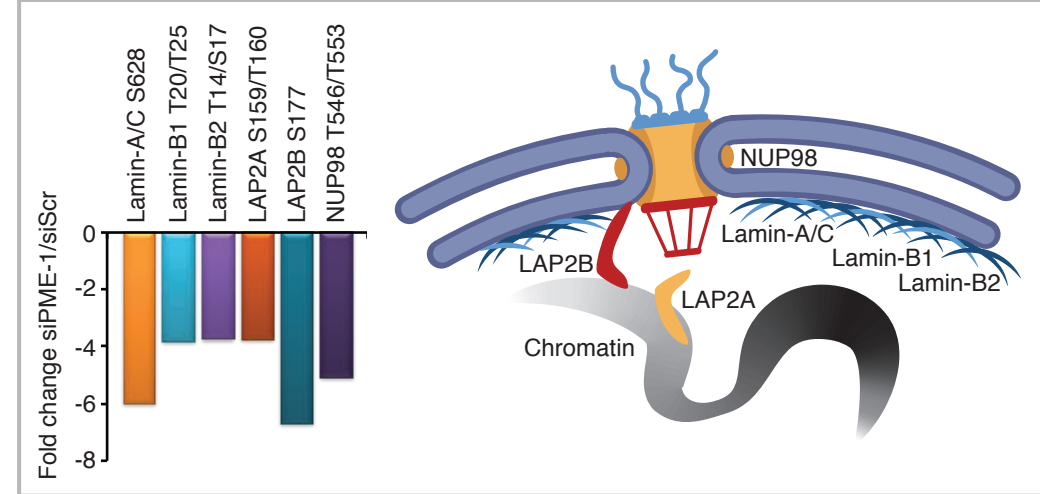


Figure 2

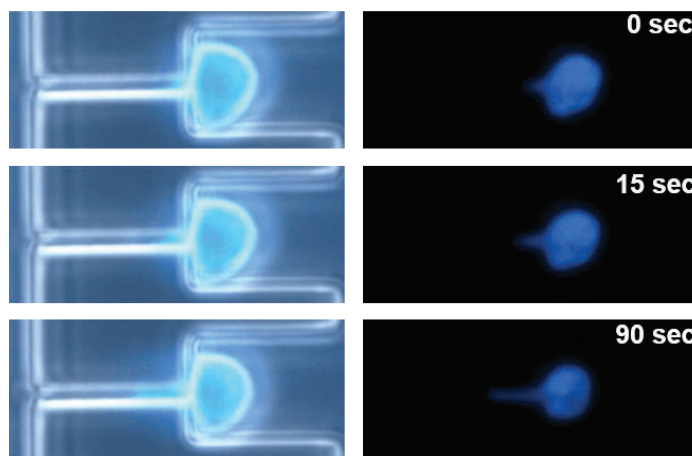
A



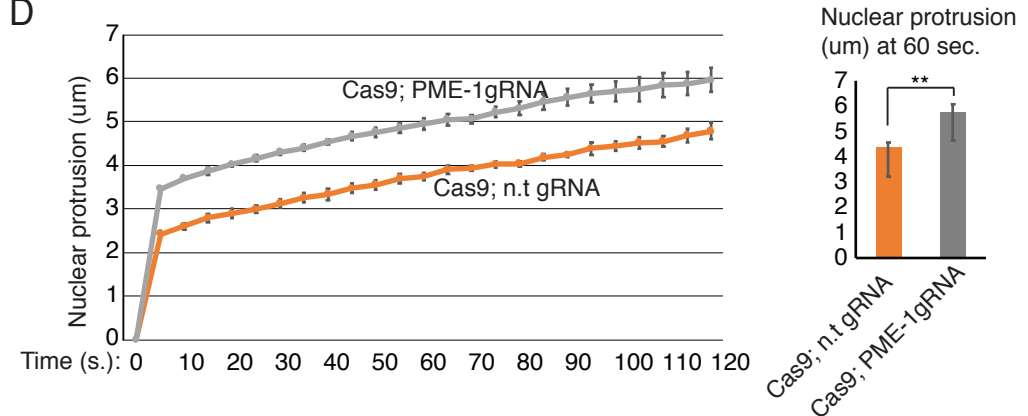
B



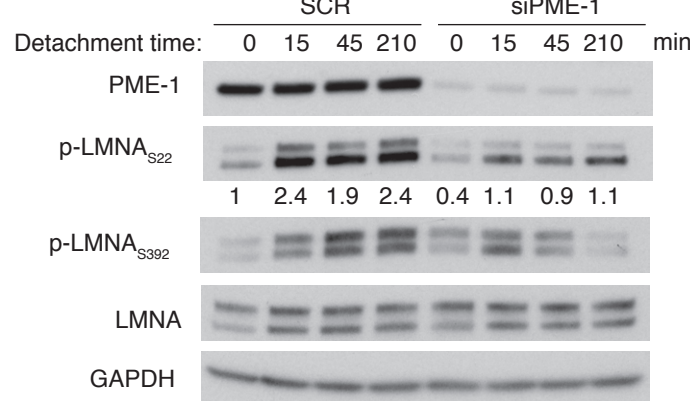
C



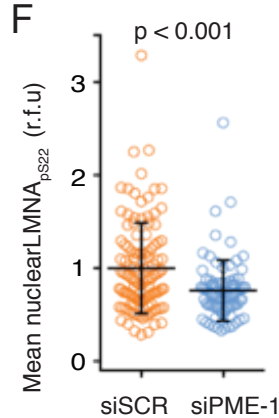
D



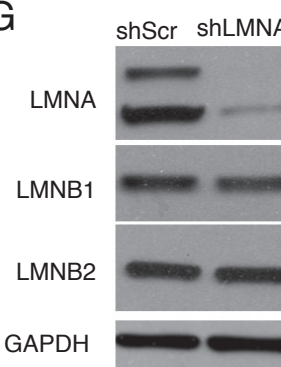
E



F



G



H

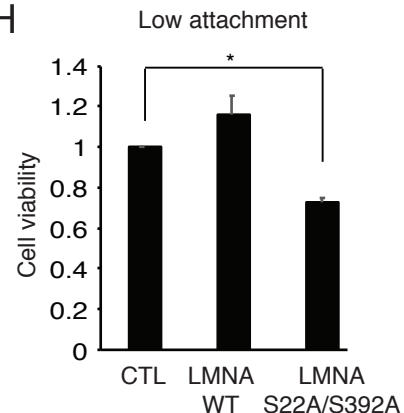
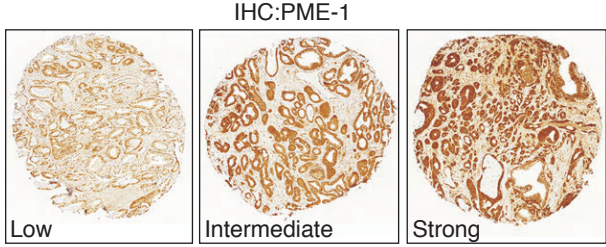


Figure 3

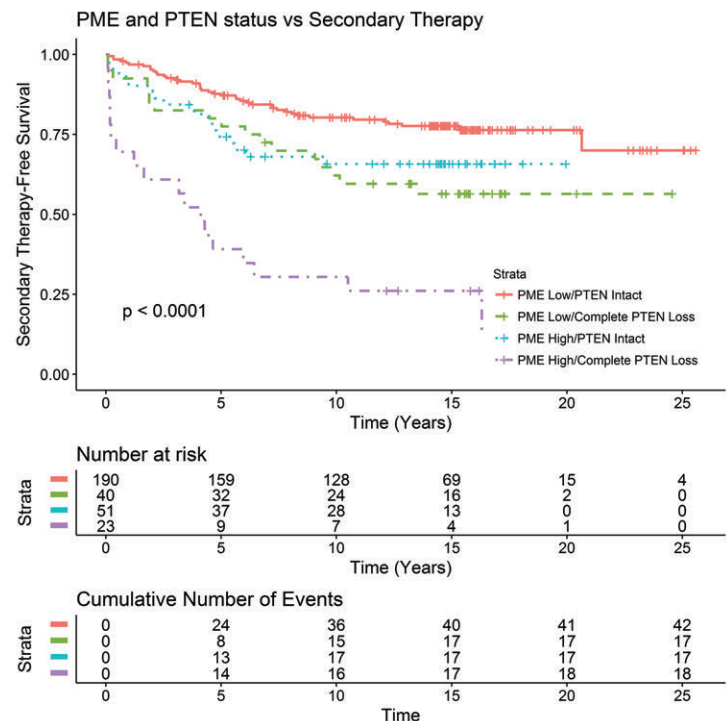
A



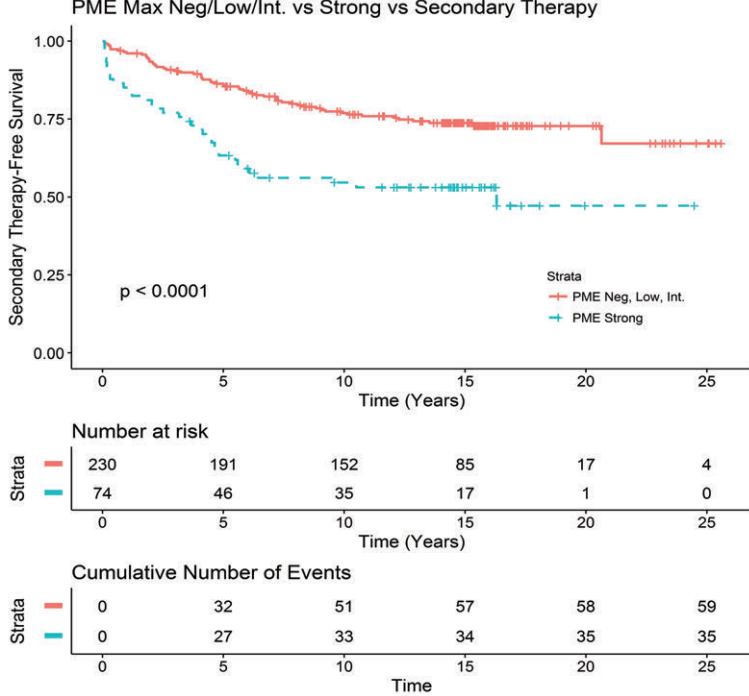
B

	PME-1 low	PME-1 high
PTEN intact	PTEN ^{Act} /PP2A ^{Act} 60.3%	PTEN ^{Act} /PP2A ^{Low} 17.8%
Complete PTEN loss	14.1%	7.8% PTEN ^{Loss} /PP2A ^{Act}

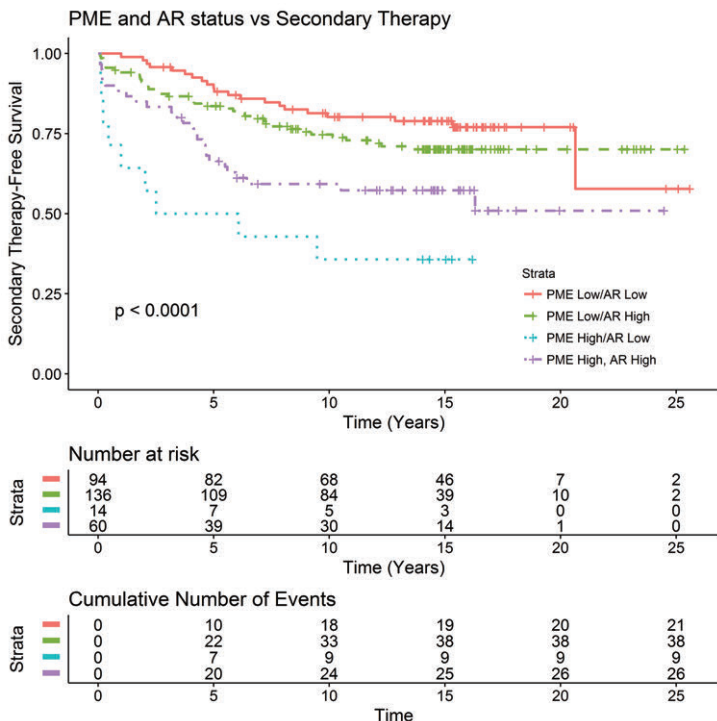
D



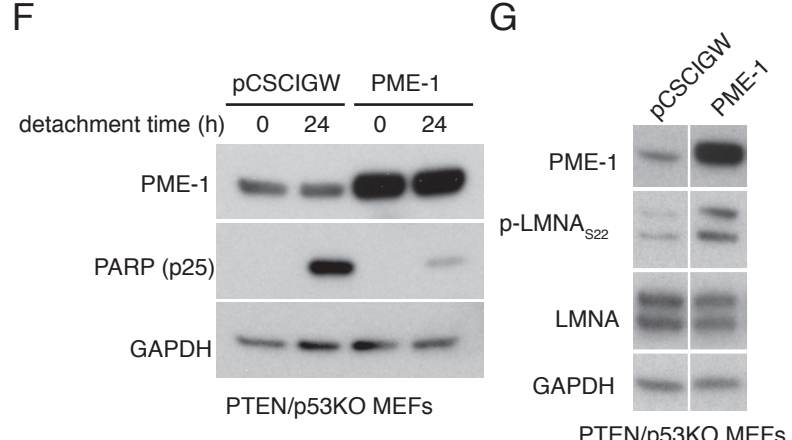
C



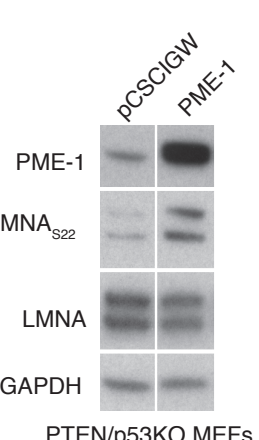
E



F



G



H

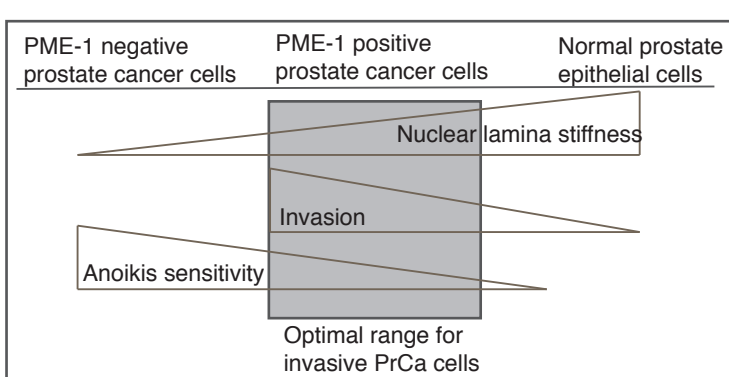


Figure 4

Table 1. Demographics of the radical prostatectomy patient cohort.

	Total Cohort (n=358)
Age at RP, years (median, IQR) (n = 358)	64.0 (59.2 – 67.9)
Preoperative PSA, ng/ml (n, %) (n = 283)	
≤10.0	143 (50.5)
10.1-20.0	89 (31.45)
>20.0	51 (18.0)
Grade group at RP (n, %) (n = 358)	
1	93 (26.0)
2	93 (26.0)
3	114 (31.8)
4	45 (12.6)
5	13 (3.6)
pT (n, %) (n = 334)	
2	202 (60.5)
≥3	132 (39.5)
Lymph node status (n, %) (n = 358)	
Negative	342 (97.2)
Positive	10 (2.8)
Follow-up time after RP, years (median, range) (n=358)	15.7 (0.7-28.6)
Death from any cause (n, %) (n = 358)	172 (48.0)
Death from prostate cancer (n, %) (n = 358)	33 (9.2)
Patients receiving secondary therapy after RP (n, %) (n = 358)	124 (34.6)

Table 2. Univariate Analysis of PME IHC and clinical variables.

	PME IHC Low (n = 238)	PME IHC High (n = 82)	P-Value
Age at RP, years (mean, SD) (n = 320)			
< 60	81 (34.0)	24 (29.3)	0.490 ^a
60 - 70	132 (55.5)	46 (56.1)	
> 70	25 (10.5)	12 (14.6)	
Preoperative PSA, ng/ml (n, %) (n = 254)			
≤10.0	100 (52.1)	32 (51.6)	1.000 ^a
10.1-20.0	59 (30.7)	19 (30.7)	
>20.0	33 (17.2)	11 (17.7)	
Grade group at RP (n, %) (n = 320)			
1	74 (31.1)	5 (6.1)	< 0.001 ^a
2	65 (27.3)	17 (20.7)	
3	73 (30.7)	36 (43.9)	
4	22 (9.2)	17 (20.7)	
5	4 (1.7)	7 (8.6)	
pT (n, %) (n = 299)			
2	150 (67.3)	28 (36.8)	< 0.001 ^a
3-4	73 (32.7)	48 (63.2)	
Lymph node status (n, %) (n = 314)			
Negative	228 (97.4)	78 (97.5)	0.974 ^a
Positive	6 (2.6)	2 (2.5)	
Secondary Therapy (n, %) (n = 320)			
No	171 (71.8)	39 (47.6)	< 0.001 ^a
Yes	67 (28.2)	43 (52.4)	
Death from any cause (n, %) (n = 320)			
Yes	104 (43.7)	46 (56.1)	0.055 ^a
No	134 (56.3)	36 (43.9)	
Death from prostate cancer (n, %) (n = 320)			
Death due to PC	20 (8.4)	11 (13.4)	0.197 ^a
Alive, or dead from other causes	218 (91.6)	71 (86.6)	

^a Fisher's exact test

440 **FIGURE LEGENDS**

441 **Figure 1. PME-1 inhibits anoikis in PTEN-deficient prostate cancer cells**

442 **A.** The effect of PME-1 depletion, utilizing two independent siRNAs, was characterized
443 by colony formation assays (10 days of growth) in two PTEN-deficient PCa cells lines
444 PC-3 and DU-145. The graphs show the quantified colony area, as mean fold change
445 +/- SD compared to siScr. N=3.

446 **B.** PME-1 knock-down effect on anchorage-independent growth in soft agar assays
447 (14 days of growth) in both PC-3 and DU-145 cells. The graphs show the quantified
448 colony area, as mean +/- S.D. fold change compared to siScr. N =2, p-value: 2-sided
449 t-test between colony areas in 15-20 image fields.

450 **C.** PME-1 inhibition effect on cell viability of PC-3 on low attachment plates, as
451 measured by Cell Titer-GLO luminescence assay. The relative cell viability was
452 calculated as compared to siScr (100%). N=2, Shown in mean + S.D, 2-sided t-test.

453 **D.** siScr and siPME-1 transfected PC-3 cells were plated 72h post-transfection on
454 normal or low attachment plates for 24h, before collection and lysis, and subsequently
455 analyzed by Western blot for cPARP induction.

456 **E.** Apoptosis induction, as measured by PARP cleavage, was studied by Western blot
457 analysis in CRISPR/Cas9 generated PC-3 cells, with and without non-targeting gRNA
458 (lanes 1-3), a pool of PME-1 gRNA transfected cells (lane 4), and a single cell subclone
459 of PME-1 targeted cells (lane 5), after 24h detachment.

460 **F.** Mechanosensitive PARP cleavage in PME-1-depleted PC-3 cells. The cells were
461 cultured on soft (0.5 kPa) or stiff (50 kPa) hydrogel for 24h before being scraped into
462 PBS, spun down, lysed and analyzed for protein expression. Results are
463 representative of two independent experiments.

464

465 **Figure 2. PME-1 supports *in vivo* anoikis resistance and survival of prostate
466 cancer cells in circulation.**

467 **A.** The effect of PME-1 effect on anchorage-independent growth of PC-3 cells *in vivo*
468 was tested by Chicken embryo chorioallantoic membrane (CAM) assay. PC-3 cells
469 were transiently transfected with either siScr or siPME-1, and 24h post-transfection
470 placed on the CAM. Growth of tumors was followed for 3-5 days.

471 **B-C.** Immunohistological stainings of dissected tumors were conducted using
472 antibodies for PME-1, VIM, TUNEL and Ki67, and subsequently the percentage of
473 TUNEL- and Ki67-positive were quantified. Shown is mean + S.E.M, p-value; Mann
474 Whitney test.

475 **D-E.** The survival of siScr and siPME-1 transfected PC-3 was studied by microinjecting
476 them into the common cardinal vein of zebrafish embryos 72h post-transfection. After
477 overnight incubation the embryos were imaged by fluorescence stereomicroscopy.
478 The number of surviving fluorescent tumor cells per was counted manually from the
479 images using FIJI and statistical analysis was performed using non-parametric
480 Kruskal-Wallis test.

481

482 **Figure 3. PME-1 associates with nuclear lamina and regulates its deformability**

483 **A.** Proximity ligation assay (PLA) was used to confirm the physical association of PME-
484 1 with Lamin-A/C in PC-3 cells. Cleraly decreased PLA signal in PME-1-1 transfected
485 cells confirm the specificity of PLA reaction. DNA was stained using DAPI

486 **B.** PME-1 depletion by transient siRNA transfection induced dephosphorylation of the
487 indicated nuclear lamina constituents in HeLa cells. Shown is Log2 fold change in
488 abundance of the indicated phosphopeptide 72 hours after transfection. Included are
489 phosphopeptides detected with 1% FDR accuracy and for which FDR for

490 reproducibility between 3 parallel samples was < 10%. The data was retrieved from
491 (28).

492 **C-D.** CRISPR/Cas9 generated control and PME-1 KO cells were analyzed by
493 micropipette aspiration, showing representative images (C) and quantification (D) of
494 nuclear protrusions (um at different time-points).

495 **E.** The effect of PME-1 knock-down in PC-3 cells on the phosphorylation of Lamin-A/C
496 S22 and S392 was confirmed by Western blot analysis, after trypsin-induced
497 detachment for the indicated time (0-210 minutes) prior to collection and lysis of
498 samples. The signal was quantified as compared to total Lamin-A/C and GAPDH.

499 **F.** Quantification depicting the phosphorylation of Lamin-A/C S22 in PME-1-depleted
500 and control PC-3 cells, 48h post-transfection and 24h after seeding on soft hydrogel
501 (2 kPa PAG). After culture the cells were fixed, stained and analyzed by confocal
502 microscopy. Mean +/- SD, Mann-Whitney test, n = 84-117 cells from two independent
503 experiments.

504 **G-H.** PC-3 cells, in which the endogenous Lamin-A/C expression was suppressed by
505 shRNA was analyzed by Western blot, and upon confirmation of Lamin-A/C
506 suppression (E) transiently transfected with either wild-type Lamin-A/C (WT) or with a
507 Lamin-A/C mutant with both serine 22 and 392 mutated to alanine (S22A/S392A). The
508 effect of Lamin-A/C phosphorylation on cell viability was analysed, as measured by
509 CellTiter-GLO assay. Shown in mean + S.D, 2-sided t-test, n=2.

510

511 **Figure 4. PME-1 overexpression associates with PTEN loss and therapy relapse
512 of PTEN negative PCa patients**

513 **A.** PME-1 protein expression in PCa tissue microarray material from 358 patients
514 treated primarily with radical prostatectomy in the Helsinki University Hospital between

515 1983 and 1998 was assessed by immunohistochemical (IHC) stainings. PME-1 protein
516 content was scored using 4-tier scale; negative (not shown), low, intermediate and
517 strong expression.

518 **B.** Assessment of the activity status of PTEN and PP2A in the patient populations by
519 using genetic deletion of PTEN and PME-1 overexpression as surrogate markers

520 **C-E.** Kaplan-Meyer analysis of time to secondary therapies after primary treatment
521 based on PME-1 status alone (C) and in combinations with PTEN deletion (D) and AR
522 expression (E).

523 **F)** Effect of stable PME-1 overexpression in anoikis in mouse embryo fibroblasts
524 (MEFs) from a PTEN/p53 KO mouse model after 24h incubation in low attachment
525 conditions. Apoptosis induction was assessed by Western blot utilizing antibodies for
526 cleaved PARP.

527 **G.** Effect of stable PME-1 overexpression in S22 phosphorylation of Lamin-A/C in
528 PTEN/p53 KO MEFs.

529 **H.** Schematic representation of prostate cell properties, such as nuclear lamina
530 stiffness, invasion and anoikis sensitivity, in relation to PME-1 protein levels and cell
531 malignancy. Based on the results and existing literature, we propose that during
532 cellular transformation nuclear lamina becomes softened to allow cell migration,
533 whereas PME-1 overexpression prevents excess softening of the lamina to the levels
534 that would threaten the viability of these cells.

535

536 **References**

- 537 1. Cao Z, Livas T, and Kyriianou N. Anoikis and EMT: Lethal "Liaisons" during
538 Cancer Progression. *Critical reviews in oncogenesis*. 2016;21(3-4):155-68.
- 539 2. Howard EW, Leung SC, Yuen HF, Chua CW, Lee DT, Chan KW, et al.
540 Decreased adhesiveness, resistance to anoikis and suppression of GRP94 are
541 integral to the survival of circulating tumor cells in prostate cancer. *Clin Exp
542 Metastasis*. 2008;25(5):497-508.
- 543 3. Yao X, Choudhury AD, Yamanaka YJ, Adalsteinsson VA, Gierahn TM,
544 Williamson CA, et al. Functional analysis of single cells identifies a rare subset
545 of circulating tumor cells with malignant traits. *Integr Biol (Camb)*.
546 2014;6(4):388-98.
- 547 4. Jamaspishvili T, Berman DM, Ross AE, Scher HI, De Marzo AM, Squire JA, et
548 al. Clinical implications of PTEN loss in prostate cancer. *Nat Rev Urol*.
549 2018;15(4):222-34.
- 550 5. Wang S, Gao J, Lei Q, Rozengurt N, Pritchard C, Jiao J, et al. Prostate-specific
551 deletion of the murine Pten tumor suppressor gene leads to metastatic prostate
552 cancer. *Cancer Cell*. 2003;4(3):209-21.
- 553 6. Vitolo MI, Weiss MB, Szmacinski M, Tahir K, Waldman T, Park BH, et al.
554 Deletion of PTEN promotes tumorigenic signaling, resistance to anoikis, and
555 altered response to chemotherapeutic agents in human mammary epithelial
556 cells. *Cancer Res*. 2009;69(21):8275-83.
- 557 7. Zheng Y, Gierut J, Wang Z, Miao J, Asara JM, and Tyner AL. Protein tyrosine
558 kinase 6 protects cells from anoikis by directly phosphorylating focal adhesion
559 kinase and activating AKT. *Oncogene*. 2013;32(36):4304-12.

- 560 8. Cariaga-Martinez AE, Lopez-Ruiz P, Nombela-Blanco MP, Motino O,
561 Gonzalez-Corpas A, Rodriguez-Ubreva J, et al. Distinct and specific roles of
562 AKT1 and AKT2 in androgen-sensitive and androgen-independent prostate
563 cancer cells. *Cell Signal.* 2013;25(7):1586-97.
- 564 9. Harada T, Swift J, Irianto J, Shin JW, Spinler KR, Athirasala A, et al. Nuclear
565 lamin stiffness is a barrier to 3D migration, but softness can limit survival. *J Cell*
566 *Biol.* 2014;204(5):669-82.
- 567 10. Rowat AC, Jaalouk DE, Zwerger M, Ung WL, Eydelnant IA, Olins DE, et al.
568 Nuclear envelope composition determines the ability of neutrophil-type cells to
569 passage through micron-scale constrictions. *J Biol Chem.* 2013;288(12):8610-
570 8.
- 571 11. Davidson PM, Denais C, Bakshi MC, and Lammerding J. Nuclear deformability
572 constitutes a rate-limiting step during cell migration in 3-D environments. *Cell*
573 *Mol Bioeng.* 2014;7(3):293-306.
- 574 12. Mitchell MJ, Denais C, Chan MF, Wang Z, Lammerding J, and King MR. Lamin
575 A/C deficiency reduces circulating tumor cell resistance to fluid shear stress.
576 *Am J Physiol Cell Physiol.* 2015;309(11):C736-46.
- 577 13. Swift J, and Discher DE. The nuclear lamina is mechano-responsive to ECM
578 elasticity in mature tissue. *J Cell Sci.* 2014;127(Pt 14):3005-15.
- 579 14. Lammerding J, Fong LG, Ji JY, Reue K, Stewart CL, Young SG, et al. Lamins
580 A and C but not lamin B1 regulate nuclear mechanics. *J Biol Chem.*
581 2006;281(35):25768-80.
- 582 15. Denais CM, Gilbert RM, Isermann P, McGregor AL, te Lindert M, Weigelin B,
583 et al. Nuclear envelope rupture and repair during cancer cell migration. *Science.*
584 2016;352(6283):353-8.

- 585 16. Butin-Israeli V, Adam SA, Jain N, Otte GL, Neems D, Wiesmuller L, et al. Role
586 of lamin b1 in chromatin instability. *Mol Cell Biol*. 2015;35(5):884-98.
- 587 17. Singh M, Hunt CR, Pandita RK, Kumar R, Yang CR, Horikoshi N, et al. Lamin
588 A/C depletion enhances DNA damage-induced stalled replication fork arrest.
589 *Mol Cell Biol*. 2013;33(6):1210-22.
- 590 18. Sangodkar J, Farrington CC, McClinch K, Galsky MD, Kastrinsky DB, and Narla
591 G. All roads lead to PP2A: exploiting the therapeutic potential of this
592 phosphatase. *FEBS J*. 2016;283(6):1004-24.
- 593 19. Westermarck J, and Hahn WC. Multiple pathways regulated by the tumor
594 suppressor PP2A in transformation. *Trends in molecular medicine*.
595 2008;14(4):152-60.
- 596 20. Kauko O, and Westermarck J. Non-genomic mechanisms of protein
597 phosphatase 2A (PP2A) regulation in cancer. *Int J Biochem Cell Biol*.
598 2018;96:157-64.
- 599 21. Kaur A, and Westermarck J. Regulation of protein phosphatase 2A (PP2A)
600 tumor suppressor function by PME-1. *Biochem Soc Trans*. 2016;44(6):1683-
601 93.
- 602 22. Khanna A, and Pimanda JE. Clinical significance of Cancerous Inhibitor of
603 Protein Phosphatase 2A (CIP2A) in human cancers. *Int J Cancer*. 2015.
- 604 23. Bluemn EG, Spencer ES, Mecham B, Gordon RR, Coleman I, Lewinshtein D,
605 et al. PPP2R2C loss promotes castration-resistance and is associated with
606 increased prostate cancer-specific mortality. *Mol Cancer Res*. 2013;11(6):568-
607 78.

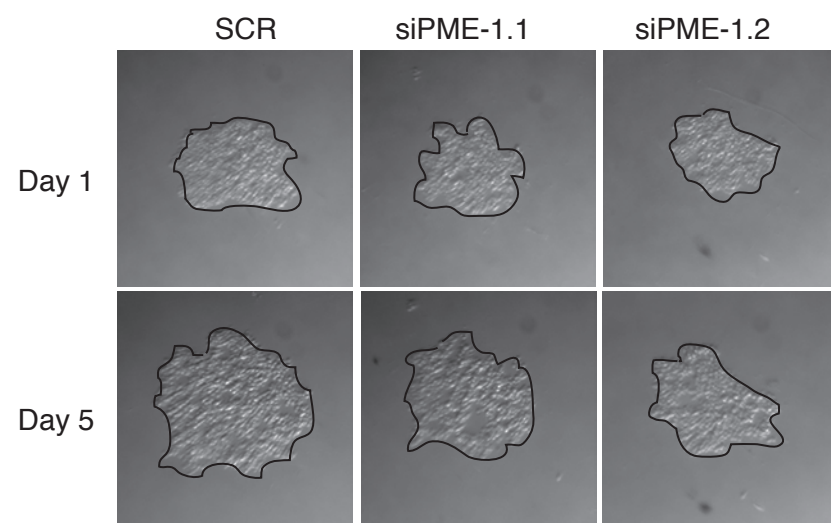
- 608 24. Liu W, Xie CC, Zhu Y, Li T, Sun J, Cheng Y, et al. Homozygous deletions and
609 recurrent amplifications implicate new genes involved in prostate cancer.
610 *Neoplasia (New York, NY)*. 2008;10(8):897-907.
- 611 25. Cheng Y, Liu W, Kim ST, Sun J, Lu L, Sun J, et al. Evaluation of PPP2R2A as
612 a prostate cancer susceptibility gene: a comprehensive germline and somatic
613 study. *Cancer Genet.* 2011;204(7):375-81.
- 614 26. Khanna A, Rane JK, Kivinummi KK, Urbanucci A, Helenius MA, Tolonen TT, et
615 al. CIP2A is a candidate therapeutic target in clinically challenging prostate
616 cancer cell populations. *Oncotarget.* 2015;6(23):19661-70.
- 617 27. Hu X, Garcia C, Fazli L, Gleave M, Vitek MP, Jansen M, et al. Inhibition of Pten
618 deficient Castration Resistant Prostate Cancer by Targeting of the SET - PP2A
619 Signaling axis. *Scientific reports.* 2015;5:15182.
- 620 28. Kauko O, Imanishi SY, Kulesskiy E, Laajala TD, Yetukuri L, Laine A, et al. Rules
621 for PP2A-controlled phosphosignalling and drug responses. *bioRxiv.* 2018.
- 622 29. Myant K, Qiao X, Halonen T, Come C, Laine A, Janghorban M, et al. Serine 62-
623 Phosphorylated MYC Associates with Nuclear Lamins and Its Regulation by
624 CIP2A Is Essential for Regenerative Proliferation. *Cell reports.*
625 2015;12(6):1019-31.
- 626 30. Pokharel YR, Saarela J, Szwajda A, Rupp C, Rokka A, Karna SKL, et al.
627 Relevance Rank Platform (RRP) for Functional Filtering of High Content
628 Protein-Protein Interaction Data. *Molecular & Cellular Proteomics.*
629 2015;14(12):3274-83.
- 630 31. Mehser H, Boudreau V, Garrido D, Bourouh M, Larouche M, Maddox PS, et al.
631 PP2A-B55 promotes nuclear envelope reformation after mitosis in Drosophila.
632 *J Cell Biol.* 2018;217(12):4106-23.

- 633 32. McClinch K, Avelar RA, Callejas D, Izadmehr S, Wiredja D, Perl A, et al. Small-
634 Molecule Activators of Protein Phosphatase 2A for the Treatment of Castration-
635 Resistant Prostate Cancer. *Cancer Res.* 2018;78(8):2065-80.
- 636 33. Patel R, Gao M, Ahmad I, Fleming J, Singh LB, Rai TS, et al. Sprouty2, PTEN,
637 and PP2A interact to regulate prostate cancer progression. *J Clin Invest.*
638 2013;123(3):1157-75.
- 639 34. Wang HB, Dembo M, and Wang YL. Substrate flexibility regulates growth and
640 apoptosis of normal but not transformed cells. *Am J Physiol Cell Physiol.*
641 2000;279(5):C1345-50.
- 642 35. Paatero I, Alve S, Gramolelli S, Ivaska J, and Ojala PM. Zebrafish Embryo
643 Xenograft and Metastasis Assay. *Bio-protocol.* 2018;8(18).
- 644 36. Jackson JB, and Pallas DC. Circumventing cellular control of PP2A by
645 methylation promotes transformation in an Akt-dependent manner. *Neoplasia*
646 (*New York, NY.* 2012;14(7):585-99.
- 647 37. Reddy S, and Comai L. Lamin A, farnesylation and aging. *Exp Cell Res.*
648 2012;318(1):1-7.
- 649 38. Mekhdjian AH, Kai F, Rubashkin MG, Prahl LS, Przybyla LM, McGregor AL, et
650 al. Integrin-mediated traction force enhances paxillin molecular associations
651 and adhesion dynamics that increase the invasiveness of tumor cells into a
652 three-dimensional extracellular matrix. *Mol Biol Cell.* 2017;28(11):1467-88.
- 653 39. Swift J, Ivanovska IL, Buxboim A, Harada T, Dingal PC, Pinter J, et al. Nuclear
654 lamin-A scales with tissue stiffness and enhances matrix-directed
655 differentiation. *Science.* 2013;341(6149):1240104.

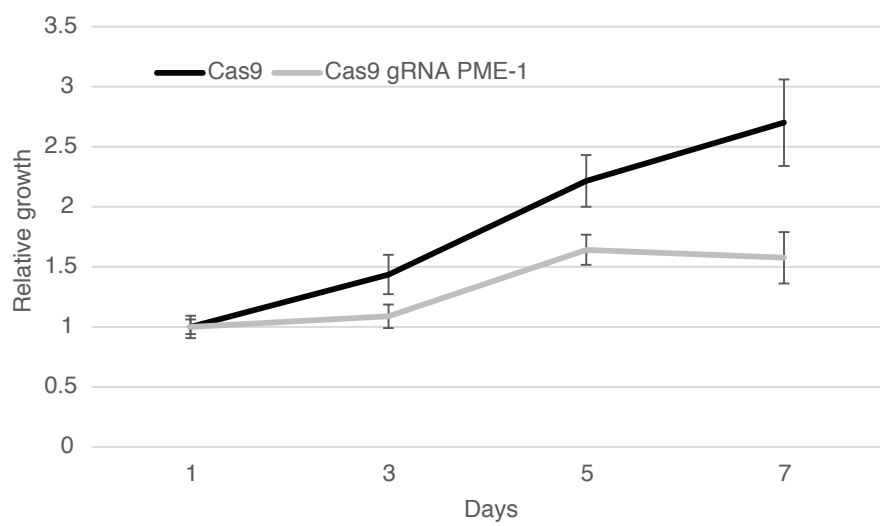
- 656 40. Kaur A, Denisova OV, Qiao X, Jumppanen M, Peuhu E, Ahmed SU, et al. PP2A
657 Inhibitor PME-1 Drives Kinase Inhibitor Resistance in Glioma Cells. *Cancer*
658 *Res.* 2016;76(23):7001-11.
- 659 41. Sahu B, Laakso M, Ovaska K, Mirtti T, Lundin J, Rannikko A, et al. Dual role of
660 FoxA1 in androgen receptor binding to chromatin, androgen signalling and
661 prostate cancer. *EMBO J.* 2011;30(19):3962-76.
- 662 42. Lahdensuo K, Erickson A, Saarinen I, Seikkula H, Lundin J, Lundin M, et al.
663 Loss of PTEN expression in ERG-negative prostate cancer predicts secondary
664 therapies and leads to shorter disease-specific survival time after radical
665 prostatectomy. *Mod Pathol.* 2016;29(12):1565-74.
- 666 43. Kaur A, Elzagheid A, Birkman EM, Avoranta T, Kytola V, Korkeila E, et al.
667 Protein phosphatase methylesterase-1 (PME-1) expression predicts a
668 favorable clinical outcome in colorectal cancer. *Cancer medicine.*
669 2015;4(12):1798-808.
- 670 44. Wen S, Niu Y, Lee SO, and Chang C. Androgen receptor (AR) positive vs
671 negative roles in prostate cancer cell deaths including apoptosis, anoikis,
672 entosis, necrosis and autophagic cell death. *Cancer Treat Rev.* 2014;40(1):31-
673 40.
- 674 45. Sato A, Hiramoto A, Satake A, Miyazaki E, Naito T, Wataya Y, et al. Association
675 of nuclear membrane protein lamin B1 with necrosis and apoptosis in cell death
676 induced by 5-fluoro-2'-deoxyuridine. *Nucleosides Nucleotides Nucleic Acids.*
677 2008;27(5):433-8.
- 678 46. Khan ZS, Santos JM, and Hussain F. Aggressive prostate cancer cell nuclei
679 have reduced stiffness. *Biomicrofluidics.* 2018;12(1):014102.

- 680 47. Naetar N, Ferraioli S, and Foisner R. Lamins in the nuclear interior - life outside
681 the lamina. *J Cell Sci.* 2017;130(13):2087-96.
- 682 48. Guzman C, Bagga M, Kaur A, Westermarck J, and Abankwa D. ColonyArea:
683 an ImageJ plugin to automatically quantify colony formation in clonogenic
684 assays. *PLoS ONE.* 2014;9(3):e92444.
- 685 49. Nowak DG, Cho HJ, Herzka T, Watrud K, DeMarco DV, Wang VMY, et al. MYC
686 Drives Pten/Trp53-Deficient Proliferation and Metastasis due to IL6 Secretion
687 and AKT Suppression via PHLPP2. *Cancer discovery.* 2015;5(6):636-51.
- 688 50. White RM, Sessa A, Burke C, Bowman T, LeBlanc J, Ceol C, et al. Transparent
689 adult zebrafish as a tool for in vivo transplantation analysis. *Cell stem cell.*
690 2008;2(2):183-9.
- 691
- 692

A



B



C

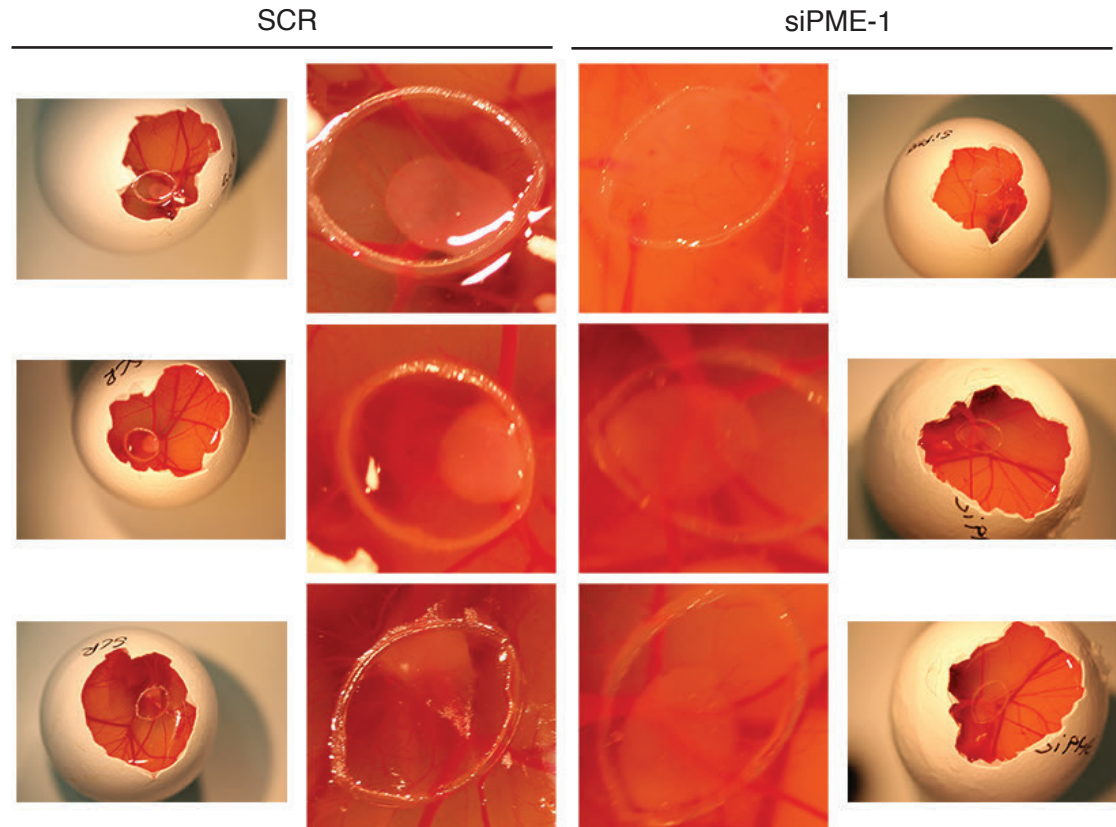


Figure S1

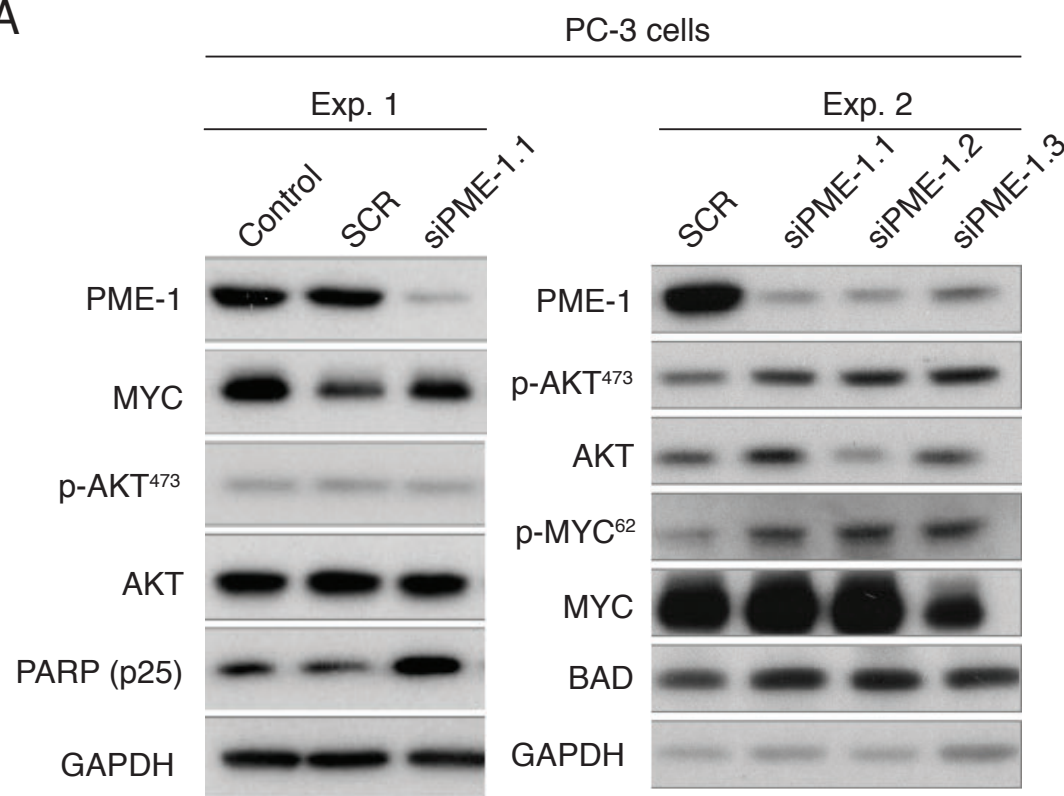
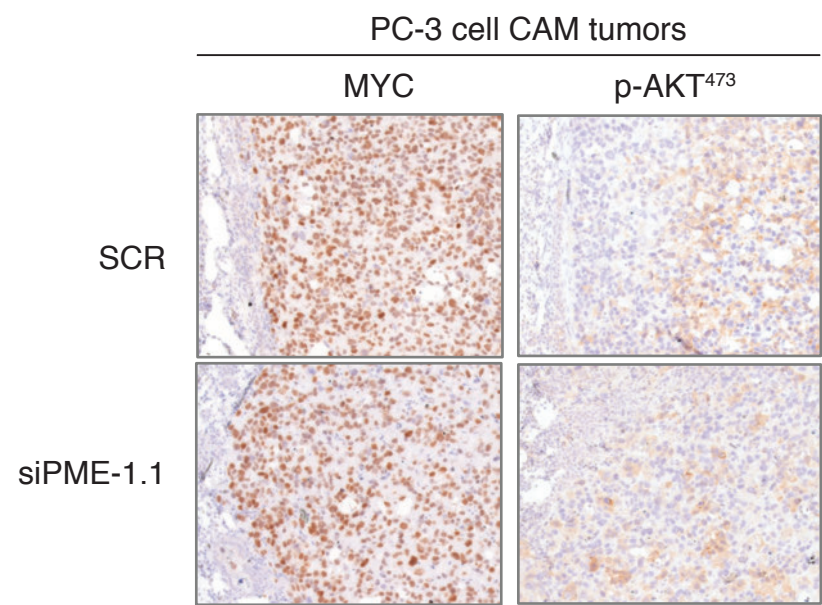
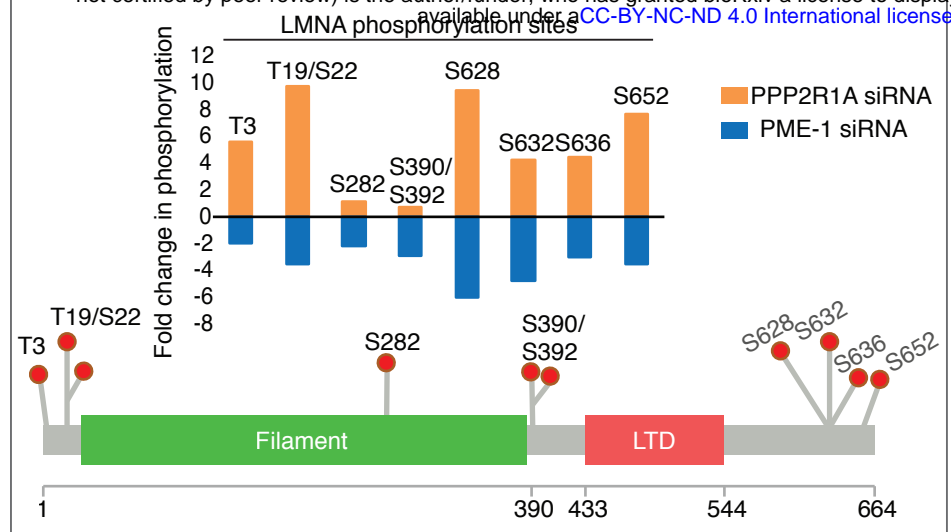
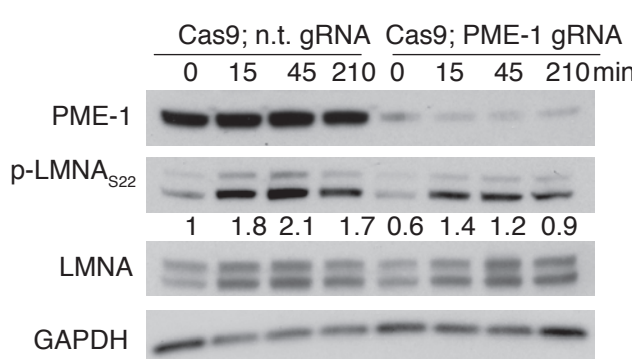
A**B**

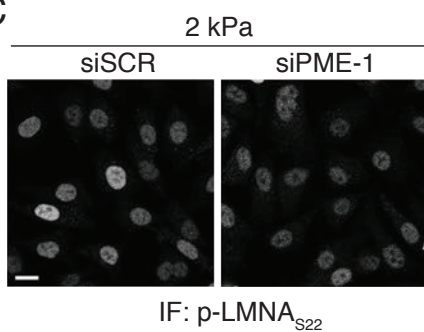
Figure S2



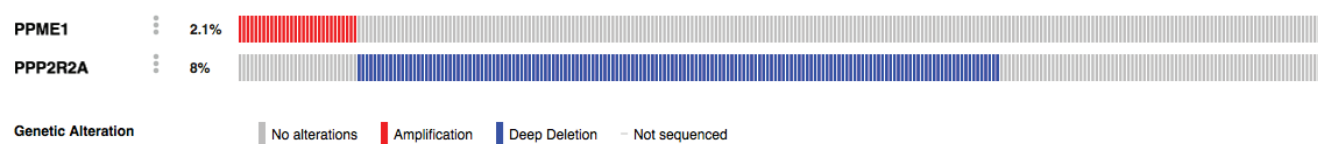
B



C

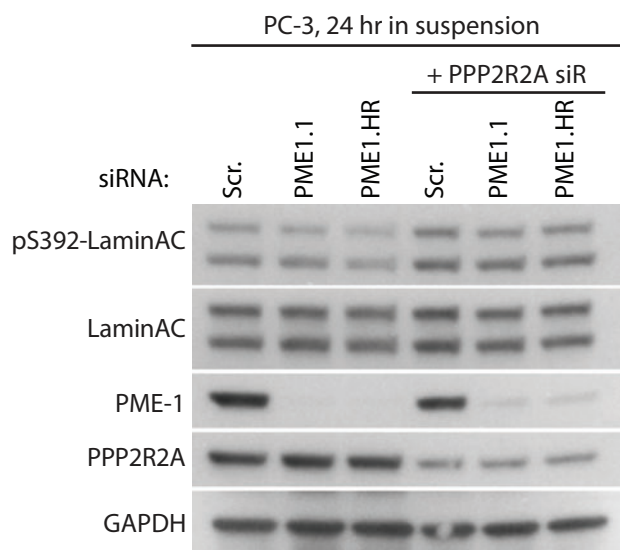


D

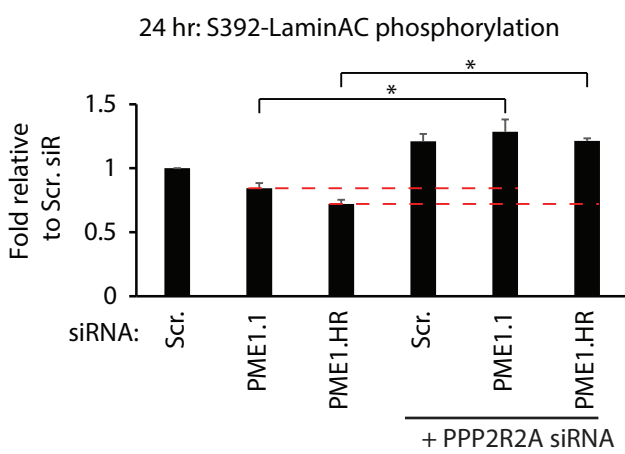


Gene A Gene B p-Value Log Odds Ratio Association
PPME1 PPP2R2A 0.106 <-3 Tendency towards mutual exclusivity

E



F



G

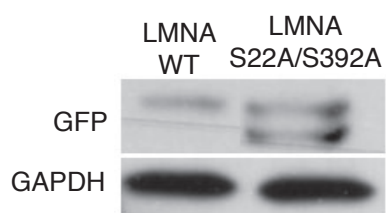


Figure S3

A

PME vs PTEN Status.

	PME Low	PME High	Total	P
PTEN Intact	193 (81.1)	57 (69.5)	250	0.043^a
Complete PTEN	45 (18.9)	25 (30.5)	70	
Total	238	82	320	

^a Fisher's exact test

PME vs AR Status.

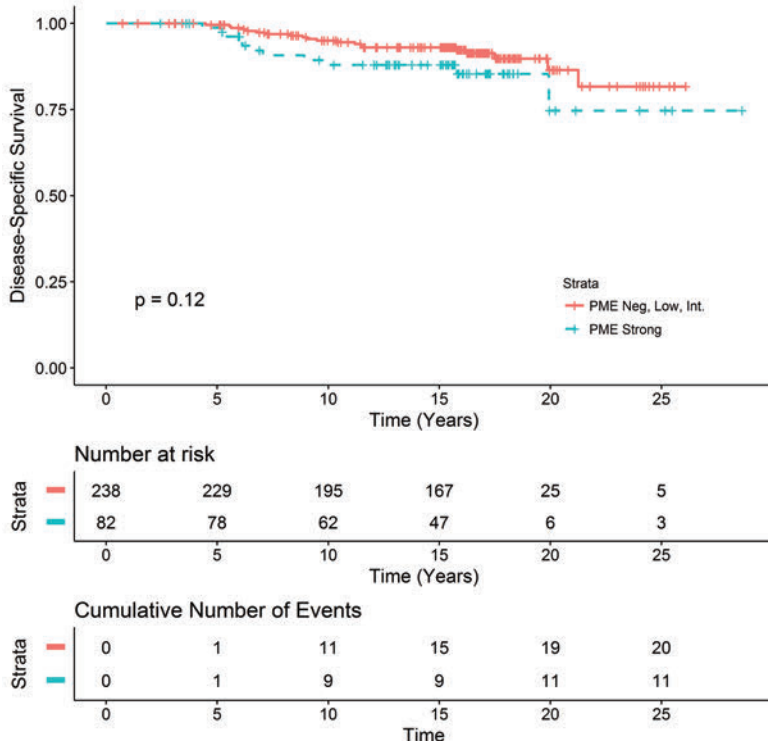
	PME Low	PME High	Total	P
AR Low	97 (40.8)	14 (17.1)	111	< 0.001^a
AR High	141 (59.2)	68 (82.9)	209	
Total	238	82	320	

PME vs ERG Status.

	PME Low	PME High	Total	P
ERG Negative	128 (53.8)	27 (32.9)	155	0.001^a
ERG Positive	110 (46.2)	55 (67.1)	165	
Total	238	82	320	

B

PME Max Neg/Low/Int. vs Strong vs Disease-Specific Survival



C

PME and ERG status vs Secondary Therapy

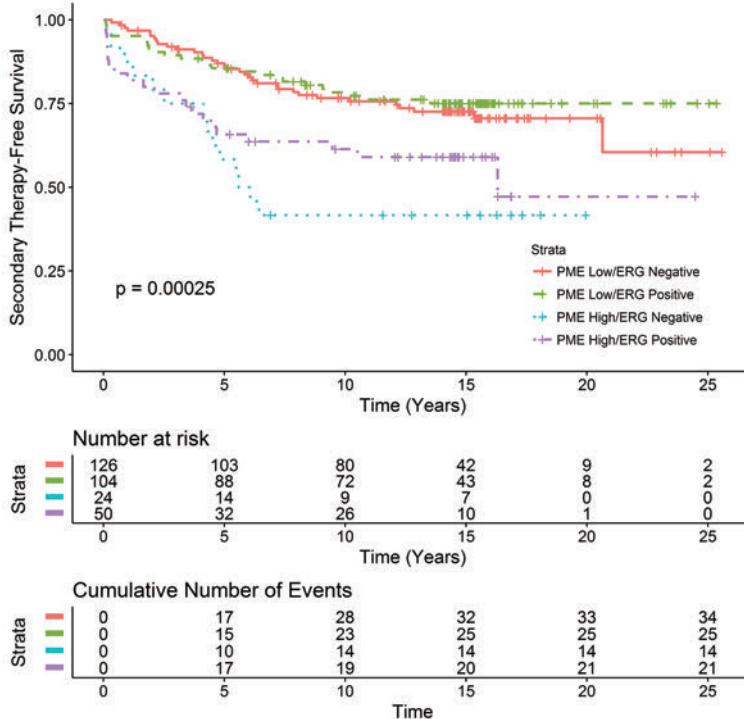


Figure S4

693

694 **SUPPLEMENTARY FIGURE LEGENDS**

695

696 **Figure S1. PME-1 supports anoikis resistance of PC-3 cells**

697 **A.** Colony growth assays of PC-3 cells were conducted on low attachment plates, after
698 PME-1 knock-down by two independent siRNAs, and the growth was compared to
699 siScr transfected cells.

700 **B.** The effect of PME-1 KO, by CRISPR/Cas9, on cell growth on low attachment plates
701 was studied for seven days.

702 **C.** Chicken embryo chorioallantoic membrane (CAM) assay was used to test the effect
703 of PME-1 on the anchorage-independent growth of PC-3 cells *in vivo*. After transient
704 transfections the cells were placed on the CAM, and the growth was followed for 3-5
705 days. The figure shows three representative pictures of siScr and siPME-1 tumors.

706

707 **Figure S2. PME-1 silencing has no effect AKT or MYC signaling in PC-3 cells *in***
vitro* or *in vivo

709 **A-B.** The effect of PME-1 silencing on AKT and MYC phosphorylation was assayed *in*
710 *vitro* by Western blot (A) and *in vivo* by immunohistochemistry on CAM tumors (B).

711

712 **Figure S3. PME-1 inhibits PP2A-mediated Lamin-A/C dephosphorylation**

713 **A.** Eight Lamin-A/C phosphopeptides/10 phospho-sites, negatively regulated by PME-
714 1 depletion and positively regulated by PP2A inhibition (siRNA targeting the scaffold
715 subunit PPP2R1A) as identified by a LC-MS/MS phosphoproteome screen (32).

716 **B.** The effect of PME-1 KO by Crispr/Cas in PC-3 cells on the phosphorylation of
717 Lamin-A/C S22 after trypsin-induced detachment. The Lamin-A/C S22 signal intensity
718 was quantified and compared to total Lamin-A/C levels.

719 **C.** Immuofluorescence analysis of phosphorylation of Lamin-A/C S22 in PME-1-
720 depleted and control PC-3 cells, 48h post-transfection and 24h after seeding on soft
721 hydrogel (2 kPa). After culture the cells were fixed, stained and analyzed by confocal
722 microscopy. Quantification of the data is shown in figure 3F.

723 **D.** Analysis of human PCa samples in cBioPortal shows loss of PPP2R2A in 8% of the
724 samples.

725 **E,F.** To show the PP2A-dependence of Lamin-A/C phosphorylation regulation by
726 PME-1, PC-3 cells were transiently depleted of PME-1 and co-depleted of the PP2A
727 B-subunit PPP2R2A. After transfection, cells were cultured on low attachment plates
728 for 24h prior to sample collection, lysis and subsequent analysis of p-Lamin-A/C, PME-
729 1 and PPP2R2A as compared to GAPDH by Western blot. (F) Relative change as
730 compared to siRNA was quantified.

731 **G.** Western blot analysis of GFP-tagged Lamin-A/C WT and S22A/S392 mutant
732 overexpression in PC-3 cells silenced for endogenous WT-Lamin-A/C.

733

734 **Figure S4. PME-1 overexpression associates with total PTEN loss in PCa**

735 **A.** PME-1 status was correlated to previously assessed PTEN, ERG and AR status.
736 PME-1 expression significantly associated with complete PTEN loss, but also with
737 ERG positivity and high AR expression status, as analysed by Fisher's exact test.

738 **B.** Association of PME-1 status and disease-specific survival in the PCa tissue
739 microarray material from 358 patients treated primarily with radical prostatectomy in
740 the Helsinki University Hospital between 1983 and 1998.

741 **C.** Kaplan-Meyer analysis of time to secondary therapies after primary treatment

742 based on PME-1 status in combination with ERG.

743

744

745 **Material and Methods**

746

747 **Cell lines**

748 PC-3 and DU-145 prostate cancer cell line were obtained from ATCC and cultured in
749 RPMI. Pten^{Δ/Δ}; Trp53^{Δ/Δ}; Isl-tdTomato mouse embryonic fibroblasts were provided by
750 Lloyd Trotmann and cultured in DMEM. All growth media were supplemented with 10%
751 heat-inactivated FBS (Biowest), 2 mmol/L l-glutamine, and penicillin (50
752 units/mL)/streptomycin (50 µg/mL; pen/strep). Cells were confirmed to be
753 mycoplasma-free and grown at 37° in a humidified atmosphere of 5% CO².

754 **siRNAs**

755 Scrambled (SCR.2): CGU ACG CGG AAU ACU UCG A
756 PME-1.1 (PME-1.3): GGA AGU GAG UCU AUA AGC A
757 PME-1.2 (PME-1 hr2): GAA UGA AAC UGG CAA GGA U
758 PP2R2A: CUG CAG AUG AUU UGC GGA U
759 Validated PP2A B-subunit siRNA was purchased from Qiagen, PME-1 siRNAs from
760 Eurofins Genomics (MWG).

761 LMNA: ON-TARGETplus human siRNA SMARTpool (L-004978-00-0005)

762 **Antibodies**

763 The following antibodies were used at the indicated dilutions: PME-1: Santa Cruz
764 Biotechnology sc-20086 (H-226) Western blotting 1:1000; PME-1: Santa Cruz
765 Biotechnology sc-25278 (B-12) Immunohistochemistry 1:1000, Immunofluorescence
766 1:100; PPP2R2A: Cell Signalling Technology #5689 Western blotting 1:1000; cleaved
767 PARP: Abcam ab32064 [E51] Western blotting 1:1000; GAPDH: Hytest 5G4-6C5
768 Western blotting 1:500.000 c-MYC: Abcam ab32072 [Y69] Western blotting 1:1000; p-
769 Myc S62:Abcam ab78318 Western blotting 1:1000; Akt1/2/3: Cell signalling #9272

770 Western blotting 1:2000; p-Akt S473: Cell Signalling Technology #4060 Western
771 blotting 1:1000; p-Akt T308: Cell Signalling Technology #13038 Western blotting
772 1:1000; Lamin A/C: Santa Cruz Biotechnology sc-20681 (H-110) Western blotting
773 1:10,000; Lamin A/C: Santa Cruz Biotechnology sc-6215 (N-18) Western blotting
774 1:1000 Immunofluorescence 1:100; Lamin A/C: Santa Cruz Biotechnology sc-7292
775 (636) Immunofluorescence 1:250; p-Lamin S22: Cell Signalling Technology #2016
776 Western blotting: 1:500 Immunofluorescence 1:50 or 1:100; p-Lamin S392: Abcam
777 ab58528 Western blotting 1:5000, Immunofluorescence 1:200

778 **siRNA/plasmid transfection**

779 For siRNA transfections Lipofectamine RNAi MAX (Thermo Fisher Scientific) was
780 used following the manufacturer's instructions. In most cases 2.5×10^5 cells were
781 seeded on a 6-well plate one day before transfection to reach 60-70% confluence.
782 Cells were then transfected with 25pmol siRNA, 7.5 μ l siRNA MAX per 6-well and
783 assayed 48-72h after transfection unless otherwise stated.

784 For plasmid transfections Lipofectamine 3000 (Thermo Fisher Scientific) was used
785 following the manufacturer's instructions. In most cases $3-4 \times 10^5$ cells were seeded
786 on a 6-well plate one day before transfection to reach 80-90% confluence. Cells were
787 then transfected with 2.5 μ g DNA, 5 μ l P3000 reagent, 3.75 μ l Lipofectamine 3000 per
788 6-well and assayed 24-48h after transfection unless otherwise stated.

789 **Colony formation assay**

790 Cells were reseeded at low confluence ($1-4 \times 10^3$) on a 12-well dish 24h after siRNA
791 transfection and grown for around 10 days to allow formation of cell colonies. Colonies
792 were then fixed with ice-cold methanol and stained with 0.2% crystal violet solution
793 (made in 10% ethanol) for 10 minutes at room temperature each. Excess stain was
794 removed by repeated washing with PBS. Plates were dried and scanned with Epson

795 perfection V700 scanner. Quantifications were performed with ColonyArea ImageJ
796 plugin (48), and graphs were plotted using the area % values.

797 **Anchorage-independent colony formation assay**

798 For the anchorage-independent colony formation assay, which correlates typically with
799 in vivo tumorigenicity, 2×10^4 cells were resuspended in 1.5ml growth medium
800 containing 0.4% agarose (4% Agarose Gel, Thermo Fisher Scientific Gibco; top layer)
801 and plated on 1ml bottom layer containing growth medium and 1.2% agarose in a 12-
802 well plate. After 14 days of growth, colonies were stained over night with 1mg/ml Nitro
803 blue tetrazolium chloride (NBT; Molecular Probes) in PBS. Colonies were imaged
804 using a Zeiss SteREO Lumar V12 stereomicroscope. Analysis was done using the
805 ImageJ software. First, the background was subtracted using the rolling ball function
806 with a radius of 50 μ m, then auto-thresholding was applied to separate the colonies.
807 Area percentage was calculated using the ImageJ built-in function 'Analyze Particles'
808 with exclusion of particles smaller than 500 μ m² that are not considered colonies.

809 **Cell viability assay on low attachment plates**

810 Cell viability on 96 Well Clear Black Round Bottom Ultra Low Attachment Spheroid
811 Microplates (Corning) was determined by using the CellTiter-Glo® Luminescent Cell
812 Viability Assay (Promega). For this purpose, a small number of cells (250-1000/well)
813 were seeded on the plates and grown for the indicated number of days. Cells were
814 then lysed in the CellTiter-Glo® reagent by vigorous pipetting and luminescence was
815 read with a Synergy H1 reader.

816 **Western blotting**

817 Western blot protein lysates were prepared in 1x RIPA buffer (150 mM sodium
818 chloride, 1.0% NP-40, 0.5% sodium deoxycholate, 0.1% SDS and 50 mM Tris, pH 7.5)
819 containing PhosSTOP™ phosphatase and cOmplete™, EDTA-free protease inhibitors

820 (Roche). The DNA in the protein samples was sheared by sonication and the protein
821 amount was estimated using the Pierce™ BCA Protein Assay Kit (Thermo Fisher
822 Scientific). Lysates were usually separated on 4–20% Mini-PROTEAN® TGX™ Gels
823 (Biorad) and transferred by wet blotting to PVDF membranes (Millipore). Unspecific
824 antibody binding was blocked with 5% non-fat dry milk in TBS-T. Incubation for most
825 of the primary antibodies was performed overnight at 4°C in either 5% non-fat dry milk
826 or 5% BSA for most of the phospho-specific antibodies. For detection, HRP- labelled
827 secondary antibodies (DAKO) followed by incubation with Pierce™ECL Western
828 Blotting Substrate (Thermo Fisher Scientific) was used.

829 **Generation of Pten^{Δ/Δ}; Trp53^{Δ/Δ} mouse embryonic fibroblasts**

830 Pten^{Δ/Δ}; Trp53^{Δ/Δ}; Isl-tdTomato MEFs were generated as previously described (49). To
831 stably overexpress PME-1 in those cells, PME-1 cDNA was cloned into pCSCIW-2
832 lentiviral construct which was then packaged into lentivirus. Following transduction,
833 GFP positive cells were sorted and overexpression of PME-1 was confirmed by
834 western blotting.

835 **CRISPR/Cas9 mediated PME-1 knock-out**

836 To generate PME-1 knock-out cells, PC-3 cells were transduced with lentivirus
837 containing lentiCas9-Blast construct (Addgene, Feng Zhang lab) and selected with
838 growth medium containing 4μg/ml blasticidin for about one week. In a second round,
839 cells were infected with lentivirus sgRNA against PME-1 exon 3 (sequence:
840 ACTTTTCGAGTCTACAAGAGTG) cloned into pKLV-
841 flipedU6gRNA_PB_BbsI_PGKpuro2ABFP construct. After puromycin selection
842 (2μg/ml in growth medium), PME-1 KO on the protein level was confirmed by western
843 blotting. Single cell clones were then obtained by single-cell sorting and the knock-out
844 was confirmed by sequencing (Primers. Forward

845 CACCGCTTTCGAGTCTACAAGAGGT; reverse

846 TAAAACGAAGATCTGTCTGCAGAAC). Cas9, non-targeting sgRNA expressing
847 cells served as a negative control in the functional assays.

848 **Chick chorioallantoic membrane (CAM) assay**

849 To start chick embryonic development for the chorioallantoic membrane assay,
850 fertilized eggs were kept rotating in an incubator at 37°C and 50-60% humidity for four
851 days. After that initial incubation time, a small hole was introduced at the sharp edge
852 of the eggs and sealed with parafilm. Following four more days of incubation on
853 stationary racks, the hole was enlarged and a plastic ring was placed on top of blood
854 vessels in the chorioallantoic membrane. Next, 1x10⁶ PC-3 cells in 20µl volume of a
855 1:1 mixture of ice-cold PBS and matrigel were pipetted inside the ring on the
856 membrane. The hole was then covered with parafilm and the eggs were incubated for
857 three more days. At day twelve of embryonic development, the animals were sacrificed
858 by freezing the eggs for 15min and the tumor cell mass was dissected from the
859 membrane and processed for further analysis.

860 **Immunohistochemistry**

861 Hematoxylin/eosin staining and immunohistochemistry were performed on 3-µm-thick
862 sections of 4% paraformaldehyde-fixed and paraffin-embedded tissues. Following
863 rehydration, endogenous peroxidase was blocked by incubation in 50% MetOH, 1%
864 H₂O₂. Subsequent antigen retrieval was performed with the 2100 Retriever (Aptum) in
865 R- Universal Buffer. Unspecific antibody binding was blocked with 10% goat serum in
866 2% BSA/PBS prior to overnight incubation at 4°C with the primary antibody. For
867 detection, the DAKO EnVision peroxidase system, followed by incubation with 0.01%
868 diaminobenzidine (Sigma-Aldrich) was used.

869 **Zebrafish *in vivo* dissemination assay**

870 The xenotransplantation of zebrafish embryos was performed as described in detail in
871 (35) with some modifications. PC-3 cells were washed with PBS, and stained with
872 CellTracker Green CMFDA dye (5uM, Thermo Fisher Scientific) and detacher and
873 detached with trypsin-EDTA in a single incubation step at +37°C. Subsequently, cells
874 were pelleted by centrifugation and washed with PBS twice. This was followed by
875 filtration through 40µM mesh into FACS tube (BD Falcon, 352235) and pelleting cells
876 by centrifugation. Finally, cells were resuspended into 30µl of injection buffer (2%PVP
877 in PBS) and kept on ice until transplanted.

878 Zebrafish (*Danio rerio*) of pigmentless casper strain (*roy*^{-/-} ; *mitfa*^{-/-})(50) was
879 used in the experiments under licence no. MMM/465/712-93 (issued by Finnish
880 Ministry of Forestry and Agriculture) and following legislation: the European
881 Convention for the Protection of Vertebrate Animals used for Experimental and other
882 Scientific Purposes and the Statutes 1076/85 and 62/2006 of The Animal Protection
883 Law in Finland and EU Directive 86/609. The embryos were obtained through natural
884 spawning, and embryos were cultured in E3-medium (5 mM NaCl, 0.17 mM KCl, 0.33
885 mM CaCl₂, 0.33 mM MgSO₄) at +33°C. At 2 or 3 days post-fertilization, the embryos
886 were anesthetized with 200mg/ml Tricaine and embedded in 0.7% low-melting point
887 agarose. Subsequently, the cell suspension was microinjected into common cardinal
888 vein (duct of Cuvier) of the embryo using glass capillaries (Transfertip), CellTramVario
889 microinjector and InjectMan micromanipulator (all from Eppendorf). Embryos were
890 liberated from the agarose gel using forceps and successfully transplanted embryos
891 were selected to the experiment. After overnight incubation at +33°C, the embryos
892 were anesthetized again with Tricaine and imaged using Zeiss StereoLumar V12
893 fluorescence stereomicroscope. The number of surviving cells was counted manually
894 from the images using FIJI and statistical analysis was performed using non-

895 parametric Kruskal-Wallis test (GraphPad Prism 6.05 software, GraphPad Software,
896 Inc.).

897 **Proximity ligation assay (PLA)**

898 Cells were grown to about 80% confluence on sterilized coverslips, fixed for 10min in
899 4% PFA and permeabilized for 10min with 0.5% Triton X-100 in TBS for proximity
900 ligation assay (PLA). The following steps were completed following the manufacturer's
901 instructions (Sigma-Aldrich). Briefly, unspecific antibody binding was blocked with the
902 provided blocking solution for 30min. The slides were then incubated with the primary
903 antibodies overnight at 4°C, with the mouse and rabbit probes for one hour at 37°C,
904 with the ligation mix for 30min at 37°C and the amplification mix for 100min at 37°C.
905 The washing steps in-between the individual steps were carried out with Buffer A
906 (Sigma), the final washing step with Buffer B (Sigma). Slides were mounted in mowiol
907 mounting medium and imaged with a Zeiss LSM780 confocal microscope.

908 **Immunofluorescence**

909 For immunofluorescence cells were fixed for 10min with 4% PFA and permeabilized
910 for 10min with 0.5% Triton X-100 in TBS. Unspecific antibody binding was blocked by
911 incubation with 10% serum from the host of the secondary antibody in 2% BSA/PBS
912 for 30min. Primary antibodies were diluted in 2% BSA/PBS and cells were usually
913 incubated with the primary antibody over-night at 4°C. As secondary antibodies
914 appropriate Alexa-Fluor conjugates (Thermo Fisher Scientific) were used at a 1:2000
915 dilution in PBS for 30min. Nuclei were stained with DAPI (4',6-diamidino-2-
916 phenylindole).

917 **Polyacrylamide hydrogels**

918 35 mm glass bottom dishes (MatTek Corporation, P35G-1.0-14-C) were treated with
919 100 µl of Bind-silane solution [7.14% Bind-silane (Sigma, M6514) and 7.14% acetic

920 acid in absolute ethanol] for 15 min, washed twice with absolute ethanol and left to dry
921 completely. A pre-polymer mix comprising 5.6% acrylamide (Sigma) and 0.078% N,N'-
922 methylenebisacrylamide (Sigma) in PBS was prepared to obtain hydrogels with an
923 elastic modulus of 1.8-2 kPa. Polymerization was initiated by adding 2.5 μ l of 20%
924 ammonium persulfate (Bio-Rad) and 1 μ l of N,N,N',N'-tetramethylethylenediamine
925 (Sigma). The solution was vortexed, 13 μ l was added on top of the glass bottom dish,
926 a 13 mm glass coverslip was placed on the drop and the gel was left to polymerize for
927 1 h at room temperature. After polymerization, the dish was filled with PBS and the
928 coverslip was carefully removed. Hydrogels were made permissive for protein binding
929 by incubating them in 500 μ l of Sulfo-SANPAH solution [0.2 mg/ml Sulfo-SANPAH
930 (Sigma, 803332) and 2 mg/ml N-(3-dimethylaminopropyl)-N'-ethylcarbodiimide
931 hydrochloride (Sigma, 03450) in 50 mM HEPES] for 30 min on slow agitation, followed
932 by a 10 min UV exposure (~30 mW/cm², 253.7 nm). Activated gels were washed three
933 times with PBS to get rid of residual Sulfo-SANPAH.
934 Alternatively, pre-activated polyacrylamide hydrogels of variable stiffness were
935 ordered from Matrigen Life Technologies. 35 mm glass bottom dishes (SV3510-EC-
936 0.5, SV3510-EC-50) were used for imaging and 6-well plates (SW6-EC-0.5, SW6-EC-
937 50) for growing cells for lysis. All hydrogels and corresponding plastic controls were
938 functionalized with bovine plasma fibronectin (Merck-Millipore, 341631) and collagen
939 type I (Sigma, C8919) by incubating the dishes in 5 μ g/ml of each protein for 1-2 h at
940 +37 °C, or overnight at +4 °C, before use.
941 For Western blot analysis from cells in hydrogels, 0.5 and 50 kPa hydrogel-coated 6-
942 well plates were immersed in cell culture medium for 30 min and seeded with 300,000
943 PME-1 or control siRNA-treated PC-3 cells per well. The cells were incubated on the
944 gels for 24 h. Once the cultures reached 80-90% confluence, the cells were washed

945 once and scraped into cold PBS, spun down and lysed in radioimmunoprecipitation
946 assay (RIPA) buffer.

947 For immunofluorescence experiments, PME-1 or control siRNA transfected cells were
948 seeded on 2 kPa hydrogel-coated glass bottom dishes and incubated for an additional
949 24 h before fixing. Cells were fixed with 4% PFA for 10 min at room temperature, and
950 simultaneously permeabilized and blocked with 0.3% Triton in 10% horse serum
951 (Gibco) for 15 min at room temperature. All samples were incubated in primary
952 antibodies overnight at +4 °C, and stained with secondary antibodies for 1-2 h at room
953 temperature on the following day. The antibodies were diluted in 10% horse serum
954 before use.

955 **Microscopy and image analysis**

956 Fluorescent specimens were imaged using a laser scanning confocal microscope
957 LSM780, controlled by Zen 2010 (Zeiss), and the objective used was a 40x/1.2 W C-
958 Apochromat objective (Zeiss). Images were analyzed using ImageJ (National
959 Institutes of Health) and CellProfiler (Broad Institute) softwares.

960